Progress in Materials Science 112 (2020) 100656

Contents lists available at ScienceDirect

Progress in Materials Science

journal homepage: www.elsevier.com/locate/pmatsci

Three-dimensional monolithic porous structures assembled from fragmented electrospun nanofiber mats/membranes: Methods, properties, and applications

Tao Xu[a], Yichun Ding[a], Zhipeng Liang[a], Hongli Sun[b], Fan Zheng[a], Zhengtao Zhu[a], Yong Zhao[c,*], Hao Fong[a,*]

[a] Program of Biomedical Engineering, South Dakota School of Mines & Technology, Rapid City, SD 57701, USA
[b] Department of Oral and Maxillofacial Surgery, College of Dentistry and Dental Clinics, University of Iowa, Iowa City, IA 52242, USA
[c] Department of Materials Science & Engineering, University of Delaware, Newark, DE 19716, USA

ARTICLE INFO

Keywords:
Electrospinning
Nanofibers
3D monolithic structures
Freeze drying
Thermally induced self-agglomeration

ABSTRACT

Three-dimensional (3D) monolithic structures (*i.e.*, aerogels/sponges/scaffolds) assembled from fragmented electrospun nanofiber mats/membranes represent an emerging research topic in the electrospinning field. Owing to extremely high porosity, as well as excellent structural flexibility and stability, these 3D nanofibrous structures have attracted significant interests for various applications. In this review, the preparation of 3D monolithic structures are thoroughly discussed; and the properties of 3D structures and their various applications in the fields of environment (*e.g.*, organic compound removal, dye adsorption, and filtration and separation), energy (*e.g.*, supercapacitor), electronics (*e.g.*, pressure sensor), chemical engineering (*e.g.*, catalyst support, thermal insulator, and Joule heater), and biomedical engineering (*e.g.*, tissue engineering, hydrogel, and drug delivery) are summarized. Additionally, the future perspectives and challenges are also presented. It is envisioned that, this review will provide important guidance in designing novel 3D electrospun nanofibrous structures and exploring their potential applications.

1. Introduction

The technique of electrospinning provides a convenient while versatile approach to make continuous nanofibers of various materials (*e.g.*, polymer, ceramic, carbon, and composite), and the resulting electrospun nanofibers possess large specific surface area, high aspect ratio, and good structual/mechanical properties. In recent decades, the electrospinning technique has attracted significant interests, primarily owing to its capability to produce fibers with ultrathin diameters (typically hundreds of nanometers) for many applications including energy, catalysis, sensor, filtration, and tissue engineering [1–9]. The electrospun nanofibers are usually collected as almost randomly overlaid mats/membranes, which generally behave like two-dimensional (2D) structures in some applications (such as tissue engineering). Until several years ago, it remained as a technological challenge to fabricate electrospun 3D nanofibrous structures with tailorable thickness, low density, high porosity, and desired mechanical properties.

Three-dimensional (3D) monolithic porous structures (*i.e.*, aerogels/sponges/scaffolds) assembled from the building blocks such as ceramics, carbons, metals, and polymers have been extensively investigated due to the appealing properties including low density,

* Corresponding authors.
E-mail addresses: yongzhao@udel.edu (Y. Zhao), hao.fong@sdsmt.edu (H. Fong).

https://doi.org/10.1016/j.pmatsci.2020.100656
Received 6 October 2019; Received in revised form 17 January 2020; Accepted 15 February 2020
Available online 17 February 2020
0079-6425/

high porosity, breathability, fast mass transfer rate, morphological/mechanical stability, and special wetting characteristics [10–15]. In the recent years, significant progress on developing electrospun 3D nanofibrous structures have been achieved. Sun and co-workers summarized the detailed advantages and disadvantages of conventional methods to produce electrospun 3D structures [16,17]. Various methods including solvent bath collection (Fig. 1A) [18], needleless electrospinning (Fig. 1B) [19], electrostatic repulsion (Fig. 1C) [20], touch-spinning (Fig. 1D) [21], thermally induced phase separation (TIPS) combined with electrospinning (Fig. 1E) [22], expanded nanofibers (Fig. 1F) [23], gas foaming (Fig. 1G) [24], and template-assisted collection (Fig. 1H) [25] have been reported to develop electrospun 3D structures with uniform small pores. However, each of these methods has some disadvantages. For example, (1) the 3D structures prepared by solvent bath collection, needleless electrospinning, and electrostatic repulsion possess poor mechanical properties, since these cotton-like 3D structures were resulted from random accumulation of nanofibers without strong binding forces; (2) the pore size of the 3D structures prepared by the methods of TIPS combined with electrospinning, expanded nanofiber, and gas-foaming is usually very small and the porosity is low, which might not be suitable for cell penetration/migration; (3) the set-up for touch-spinning is complicated; and (4) the 3D structure made from template-assisted collection is hollow/tubular shape, which may not behave as 3D substrate in some applications. To improve the pore size and porosity, several methods including rapid prototyping combined with electrospinning (Fig. 1I) [26], femto-second laser combined with electrospinning (Fig. 1J) [27], direct-writing electrospinning with stabilized jet (Fig. 1K) [28], electrospun nanofibrous yarns (Fig. 1L) [29], and self-assembly of electrospun nanofibers (Fig. 1M) [30] have been explored. Nevertheless, these methods are time-consuming and the device set-ups are often complicated; moreover, the mechanical properties and pore structures need further improvements.

Inspired by the conventional assembly of building blocks (*e.g.*, carbon nanotubes and graphene nanosheets) to fabricate functional aerogels/sponges, Ding's group [31] reported the 3D electrospun nanofibrous aerogels made from the building blocks of shortened electrospun nanofibers in 2014, in which homogenized short electrospun nanofibers were used as the building blocks for the construction of 3D structures *via* freeze-drying approach (as shown in Fig. 2). The obtained 3D nanofibrous structures possessed desired hierarchal pores and structural flexibility, leading to low density and high porosity. Shortly thereafter (in 2015), Greiner's group [32] and our group [33] also reported the fabrication and application of 3D electrospun nanofibrous structures. These reports provided a simple while efficient method to convert quasi 2D electrospun nanofiber mats/membranes into genuine 3D monolithic porous structures, thus leading to numerous cutting-edge research activities. Owing to extremely low density, very high porosity, and excellent structural flexibility/stability, these innovative 3D nanofibrous structures have attracted growing interests for different applications; hence, it is necessary and crucial to give a comprehensive review about this newly rising topic area.

In this review, we have thoroughly summarized the methods, properties, and applications of these 3D monolithic porous structures assembled from fragmented electrospun nanofiber mats/membranes. In particular, we have discussed about two approaches (*i.e.*, freeze drying and TISA methods) for the development of electrospun 3D nanofibrous structures, the unique properties, and various applications in fields of environment (*i.e.*, organic compound removal, dye adsorption, and filtration and separation), energy (*i.e.*, supercapacitor), electronic (*i.e.*, pressure sensor), chemical engineering (*i.e.*, catalyst carrier, thermal insulator, and Joule heater), and biomedical engineering (*i.e.*, tissue engineering scaffold, hydrogel, and drug delivery). Additionally, future perspectives and challenges are also described. It is envisioned that, this review will provide essential guidance in designing novel 3D electrospun structures and exploring their potential applications.

2. Methods to assemble 3D monolithic porous structures from fragmented electrospun nanofiber mats/membranes

2.1. Freeze drying method

2.1.1. Formation mechanism

Freeze drying (or lyophilization) is a dehydration process, in which the frozen solvent in a substance sublimes directly from the solid phase to the gas phase under reduced surrounding pressure (*i.e.*, under vacuum). In 2006, Deville *et al.* [34] demonstrated that the physics of ice formation can be used to develop sophisticated porous and layered-hybrid materials. Since then, the freeze drying technique has been widely adopted to fabricate 3D aerogels/sponges/scaffolds of carbon nanofibers (CNFs) [10], carbon nanotubes (CNTs) [11], graphene and graphene oxide (GO) [35,36], nanocellulose [37,38], ceramic [39–41], metal [42,43], and biopolymer [44]. It is important to note that Ding's group [31] first reported to use fragmented/shortened electrospun nanofiber mats/membranes as the building blocks for making 3D aerogels *via* freeze drying.

Fig. 3 shows the formation mechanism of interconnected and hierarchically structured pores of 3D aerogel *via* freeze drying. During the freezing step, the homogenized/dispersed nanofibers are enriched among the solvent crystals. With the growth of crystals, the nanofibers are confined among the crystals and become entangled because of the expansion of crystals. Eventually, the nanofibers are locked into a 3D solid network. In the subsequent drying step, the solidified solvent sublimes, and the electrospun 3D nanofibrous sponge/aerogel is obtained. The structure of this 3D sponge is a replica of that solidified solvent, and the large pores are determined by the solidified solvent crystals; while the small pores are resulted from the shortened/fragmented electrospun nanofiber mats/membranes.

2.1.2. Dispersion medium

A dispersion medium contains shortened nanofibers, dispersion solvent, and binding agent, each of which plays an improtant role in the formation of 3D structures. Judiciously selecting the dispersion medium is the key to fabricate ideal 3D strucutres for different applications.

Electrospinning can produce various types of nanofibers including polymer, ceramic, carbon, and composite; in principle, all of

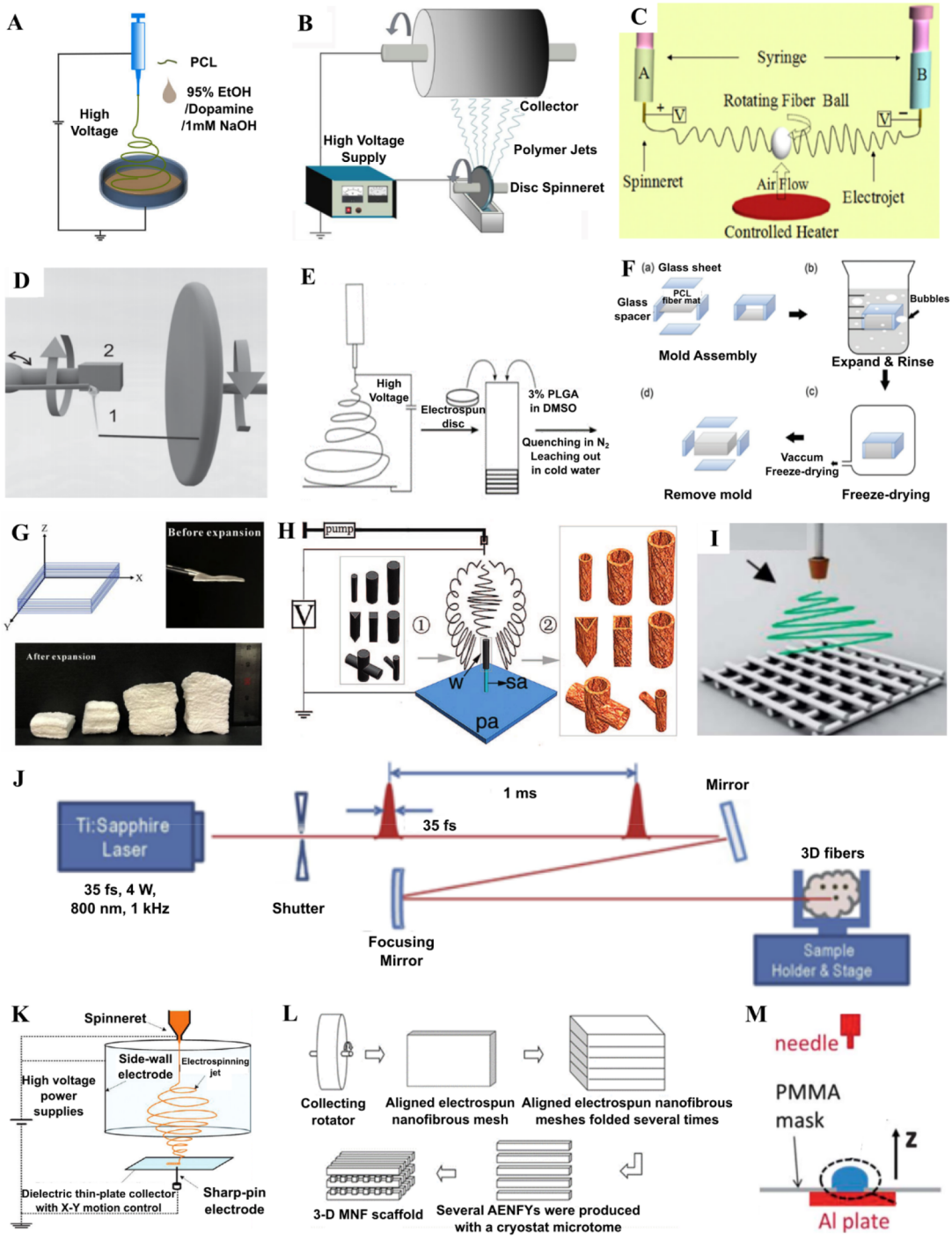

Fig. 1. Schematic diagrams showing different methods for the fabrication of electrospun 3D structures, including (A) solvent bath collection, reproduced with permission from (2016) ACS [18], (B) needleless electrospinning, reproduced with permission from (2014) Elsevier [19], (C) electrostatic repulsion, reproduced with permission from (2016) Elsevier [20], (D) touch-spinning, reproduced with permission from (2015) Wiley [21], (E) TIPS combined with electrospinning, reproduced with permission from (2013) Elsevier [22], (F) expanded nanofiber, reproduced with permission from (2016) Wiley [23], (G) Gas foaming, reproduced with permission from (2019) Elsevier [24], (H) Template-assisted collection, reproduced with permission from (2008) ACS [25], (I) rapid prototyping combined with electrospinning, reproduced with permission from (2014) RSC [26], (J) femtosecond laser combined with electrospinning, reproduced with permission from (2014) Elsevier [27], (K) direct-writing electrospinning with stabilized jet, reproduced with permission from (2012) ACS [28], (L) electrospun nanofibrous yarns, reproduced with permission from (2012) Wiley [29], and (M) self-assembly of electrospun nanofibers, reproduced with permission from (2013) RSC [30].

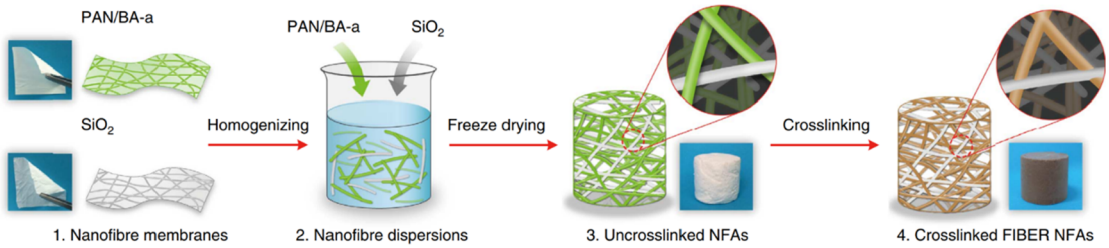

Fig. 2. A schematic representation showing the synthetic steps of fibrous, isotropically bonded elastic reconstructed 3D nanofibrous aerogels (NFAs). (1) Flexible PAN/BA-a and SiO_2 nanofiber membranes are produced by electrospinning. (2) Uniform nanofiber dispersions are fabricated *via* high-speed homogenization. (3) Uncrosslinked NFAs are prepared by freeze drying nanofiber dispersions. (4) The resultant FIBER NFAs are prepared by the crosslinking treatment. Reproduced with permission from (2014) Nature Publishing Group [31].

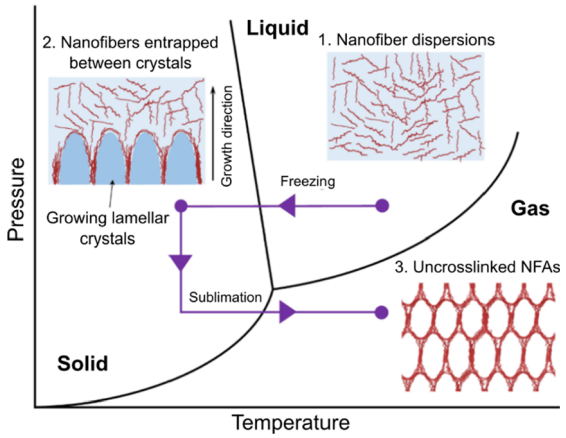

Fig. 3. Mechanism for the formation of hierarchical cellular structure. Reproduced with permission from (2014) Nature Publishing Group [31].

electrspun nanofibers can be utilized as building blocks to fabricate into 3D structures. For selecting nanofiber materials, the properties (such as chemical, mechanical, thermal, and surface properties) should be carefully considered upon different applications. For example, polyacrylonitrile (PAN) [45] has been selected as the nanofiber material for making 3D carbon structures, because PAN is the most commonly used polymer precursor to produce carbon fibers. Additionally, silica (SiO_2) nanofibers [31] and polyimide (PI) nanofibers [46] have been adopted to make flexible and elastic 3D structures because of their excellent mechanical properties; while PI nanofibers [47] with outstanding thermal stability has also been chosen for the fabrication of thermal insulation materials. Poly(bis (benzimidazo)benzophenanthroline-dione) (BBB) [48], a rigid-rod ladder type polymer with aromatic and heterocyclic rings in the macromolecular backbone, has been selected to prepare high temperature stable, intrinsic flame retardant sponge. Biomass such as cellulose [49] has been used to develop 3D sponges due to its recyclability and renewability. Biomaterials such as polycaprolactone (PCL) [33], polylactic acid (PLA) [50], and gelatin [51] have been studied to develop tissue engineering scaffolds, since they are biocompatible and biodegradable.

To fragment/shorten electrospun nanofiber mats/membranes, a homogenizer such as a high-speed blender is commonly adopted, while the size of fragmented mats/membranes and the length of shortened nanofibers are primarily determined upon the properties of different types of nanofibers and mats/membranes, as well as the vigorousness and duration of homogenization process. With the length of shortened nanofibers in the range from tens to hundreds of micrometers, the assembled 3D structures generally have good integrity after freeze drying; on the other hand, if the length is merely a few micrometers, it is difficult to make 3D structures with good morphological integrity/stability. Additionally, the properties of nanofibers are also important on the length of shortened/fragmented nanofibers. For example, most polymers such as PAN and PI are soft, thus the shortened nanofibers have relatively long length; while PAN-derived CNFs are relatively brittle, which leads to short nanofibers. As shown in Fig. 4A and B, the average lengths of the shortened PAN and CNFs are approximately 112.6 μm and 2.2 μm, respectively.

The dispersion solvent/medium for making the resulting suspension has an important impact on the formation of morphologically/structurally stable 3D structure, and the melting point is a key criterium for selecting the solvent. Water (with the melting point of 0 °C) is commonly selected as low-cost freeze drying solvent, while other organic solvents such as dioxane (12 °C), DMSO (19 °C), *tert*-butanol (~25 °C), and camphene (~50 °C) can also be selected. Although water is a common solvent/medium for freeze drying, relatively large and non-uniform ice crystals are formed at the slow freezing rate of 0.5–3 °C min^{-1}, resulting in cracks on both outer and inner surfaces, as well as poor integrity of the 3D structure. The size and uniformity of ice crystals could be appreciably improved upon adding a small amount of ethanol in the suspension, even though ethanol alone is not a good solvent for freeze drying (due to low melting point) [46]. Evidently, those organic solvents which are suitable for freeze drying can also be used to adjust the size and

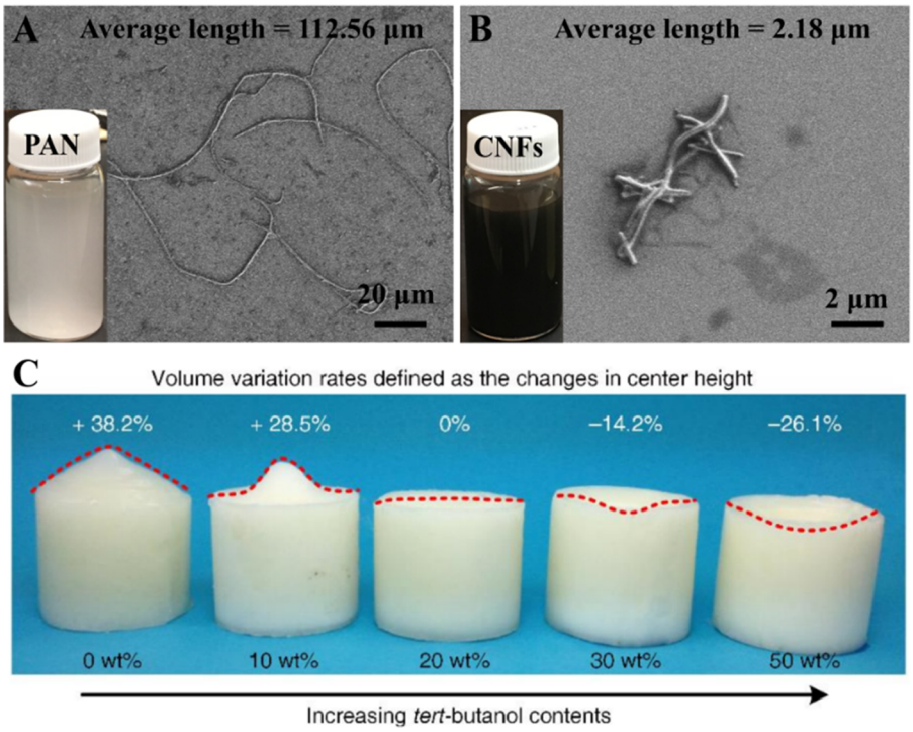

Fig. 4. SEM images showing the shortened electrospun nanofibers of (A) PAN and (B) CNFs. Insets: photos showing the nanofiber dispersed in water. Reproduced with permission from (2017) RSC [46]. (C) Photograph showing the frozen nanofiber dispersions with different concentrations (wt%) in *tert*-butanol. The top values indicating the volume variations (defined as the changes in center height of the relevant frozen cylinders). Reproduced with permission from (2014) Nature Publishing Group [31].

uniformity of ice crystals. For example, *tert*-butanol [31] can be mixed with water to control the volume and/or shape of the frozen samples, as shown in Fig. 4C.

2.1.3. Binding agent

The solid network in a 3D structure composed of shortened nanofibers alone is usually fragile after freeze drying due to lack of strong bonding/interaction among the shortened nanofibers (*i.e.*, only topological entanglements and weak Van de Waals interactions are present). Therefore, crosslinking/binding agents are usually added to strengthen 3D structures. The following four methods have been used for the addition of crosslinking/binding agents: (1) Add the crosslinking agent directly into polymer solution before electrospinning. For example, BAF-a [31] was added into PAN solution before electrospinning (Fig. 5A1 & A2). (2) Add the binding agent such as poly(amic acid) (PAA) [47], glutaraldehyde [51], konjac glucomannan (KGM) [52], alginate/Al^{3+} [53], GO [54], citric acid [55], or poly(vinyl alcohol) (PVA) [46] into the dispersion solvent during the preparation of nanofiber suspension (which has been the most commonly adopted method to date). For example, to improve the mechanical integrity and elasticity of 3D regenerated cellulose (RC) nanofibrous sponge, PVA was used as the binding agent; and it was added into the nanofiber suspension before freeze drying [46]. During the stabilization at ~230 °C, PVA macromolecules would undergo chemical changes to form dehydrated structures [56–58], which could conglutinate/bond nanofibers together in the 3D structure (Fig. 5B1 & B2). (3) Use UV crosslinkable copolymer for making nanofibers. For example, poly(MA-co-MMA-co-MABP) (PMMM) [32] was synthesized from MA, MMA, and MABP by free radical copolymerization (Fig. 5C1 & C2); thereafter, the PMMM nanofibers in 3D structure would fuse together upon UV irradiation. Additionally, photo-crosslinkable poly(N-isopropyl acrylamide) (PNIPAM) [59] was also studied to fabricate the mechanically stabilized sponges. And (4) thermally induced intermolecular condensation [60], in which macromolecules undergo crosslinking at elevated temperature and further conglutinate the skeleton of PI nanofiber aerogels without using crosslinkers (Fig. 5D1 & D2). The thermally induced intermolecular condensations would occur uniformly in the entire networks/structures thus form strong covalent bonding at the interfaces among nanofibers. Recently, PI nanofibers have been conglutinated at their cross-points *via* a controllable manner using the solvent-vapor [61], and the resulting aerogels have superelasticity. This method does not involve chemical crosslinking and/or thermal treatment, thus it can considerably mitigate the morphological and structural variations.

2.1.4. Modification and functionalization

To provide additional properties to 3D aerogels/sponges, functional fillers can be incorporated into the 3D structures; and the functionalizations are typically achieved through attaching the fillers to the surfaces of nanofibers. For example, SiO_2 nanoparticles

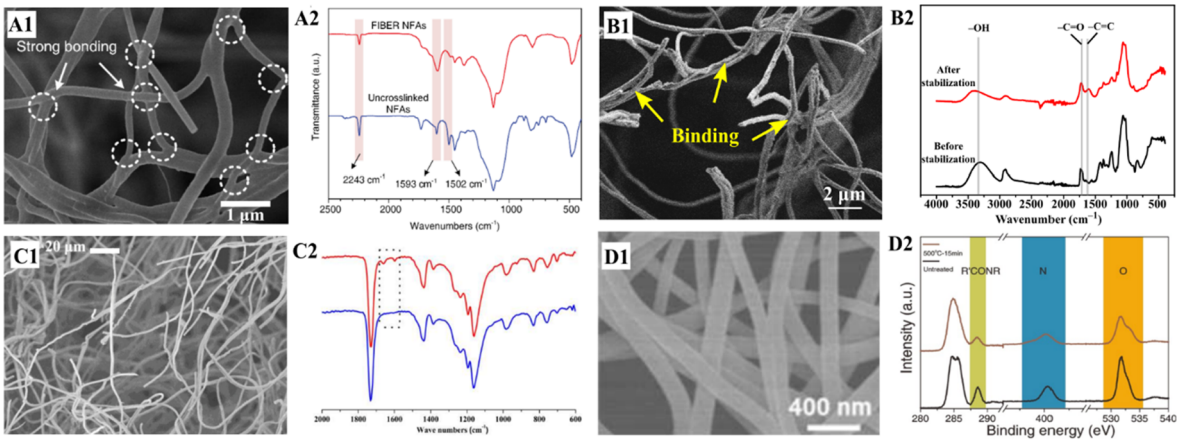

Fig. 5. (A1) The FIBER NFAs had obvious crosslinked 3D fibrous networks with strong bonding among the fibers (A2) FT-IR spectra of uncrosslinked NFAs and FIBER NFAs. Reproduced with permission from (2014) Nature Publishing Group [31]. (B1) SEM image showing the binding of RC nanofibers with PVA. (B2) FT-IR spectra acquired from UECS before and after stabilization at ~230 °C. Reproduced with permission from (2018) Elsevier [49]. (C1) SEM image showing the binding of poly(MA-MMA-MABP). (C2) ATR-IR spectra of poly(MA-MMA-MABP) before and after crosslinking upon UV irradiation. Reproduced with permission from (2015) Wiley [32]. (D1) SEM images of PINFA bound by thermally induced intermolecular condensation. (D2) XPS spectrum of PINFAs and un-PINFAs. Reproduced with permission from (2017) RSC [60].

[62] were added to achieve super-hydrophobicity of PAN/SiO_2 aerogel (Fig. 6A); CNFs [46] (Fig. 6B) and Ag nanowires [63] (Fig. 6C) were incorporated to improve the electrical conductivity of the sponge; Au nanoparticles [64] were *in situ* immobilized on the nanofiber surface (Fig. 6D) and provided the sponge with the good catalytic ability; Halloysite nanotubes (HNTs) [65] were supported by the nanofibers (Fig. 6E) and the resulting sponge demonstrated high performance as innovative dye adsorbent and catalyst support. Ketjen carbon nanoparticles [66] (Fig. 6F) were combined with short PI fibers and the fabricated PI-carbon sponges not only had high mechanical properties but also retained low thermal conductivity even in comparison with pristine PI sponges. Other functional fillers including nanoporous lignin-based CNFs, magnetic nanoparticles, noble metal nanoparticles, and photocatalytic nanoparticles are also expected to render 3D structures with specific functions.

In addition to the incorporation of nanofillers, the chemical modification on the surface of nanofibers can also expand the applications of 3D structures. For example, Duan et al. coated poly(p-xylylene) (PPX) onto sponges by chemical vapour deposition (CVD, as shown in Fig. 6G1 & 6G2) [67]. PPX is a hydrophobic polymer that is highly suitable for coating applications, because it possesses advatageous properties including strong adhesion to other materials, excellent chemical resistance, good biocompatibility, and high thermal stability. Upon varying the coating thickness, PPX modified sponges exhibited tunable properties including density, water contact angle (*i.e.*, hydrophilicity), solvent resistance, and mechanical properties.

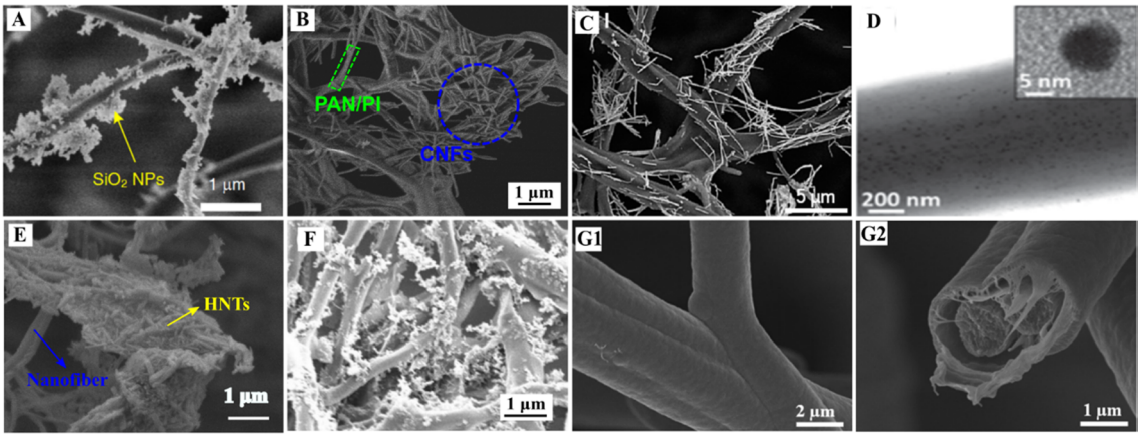

Fig. 6. (A) SEM image of FIBER aerogel, showing the hierarchical cellular fibrous structure and SiO_2 NPs. Reproduced with permission from (2015) ACS [62]. (B) SEM image of the 3D conductive sponge with CNFs-to-PAN/PI of 1:3. Reproduced with permission from (2017) RSC [46]. (C) SEM image of the PIS/AgNW sponge. Reproduced with permission from (2017) ACS [63]. (D) TEM image of AuNPs (3.56 wt%.) immobilized on a nanofiber in sponge and the inset showing an individual AuNP. Reproduced with permission from (2016) Wiley [64]. (E) SEM image acquired from HNTs sponge with the weight ratio of nanofibers-to-HNTs being 1:8. Reproduced with permission from (2019) Elsevier [65]. (F) SEM image of PI-carbon nanoparticle sponge. Reproduced with permission from (2019) Elsevier [66]. (G1-G2) SEM images showing a sponge coated with 1.0 μm PPX (G1) and the corresponding cross section (G2). Reproduced with permission from (2016) RSC [67].

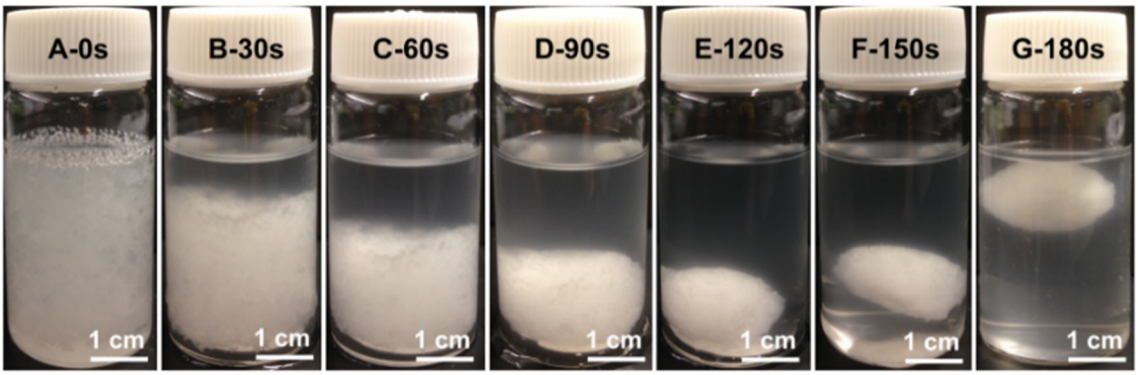

Fig. 7. A series of photographs showing the formation of PCL 3D nanofibrous agglomerate *via* the TISA process: (A) uniform suspension of short nanofibers and tiny pieces of PCL before thermal treatment; and the suspension after being heated at 55 °C for (B) 30 s, (C) 60 s, (D) 90 s; (E) 120 s, and (F) 150 s, respectively; and (G) the obtained agglomerate after thermal treatment for 180 s (note that the bottle was submerged in ice water immediately thereafter.) Reproduced with permission from (2015) Wiley [33].

2.2. Thermally induced self-agglomeration (TISA) method

2.2.1. Formation mechanism

Our research group has developed an innovative method (*i.e.*, the TISA method) to assemble shortened/fragmented PCL nanofiber mats/membranes into 3D scaffolds [33]. Upon submerging the uniformly dispersed short nanofibers and tiny pieces of PCL into a water bath at a temperature close to the PCL melting point (*e.g.*, 55 °C), these building blocks would spontaneously agglomerate into a 3D structure with interconnected and hierarchical pores; and the subsequent freeze drying would result in the formation of morphologically/structurally stable 3D nanofibrous scaffolds. Rather than using additional binding agents, PCL itself was able to bind/fuse nanofibers. The formation of PCL 3D nanofibrous agglomerate *via* the TISA process was recorded by a digital camera with an interval of 30 s, as shown in Fig. 7. Prior to the thermal treatment (Fig. 7A), short nanofibers and tiny pieces of PCL were uniformly dispersed in the suspension. Upon submerge of the glass bottle into a water bath at 55 °C for 180 s, the PCL nanofibers gradually self-agglomerated and formed a stable 3D nanofibrous structure (Fig. 7B–G). This is because the melting point of PCL is 60 °C, and the surface of PCL nanofibers become soft/sticky at 55 °C. Immediately afterward, the bottle was taken out of the water bath and submerged in ice water to prevent further shrinkage and/or agglomeration (Fig. 7G). Compared to the scaffolds prepared *via* the conventional freeze-drying (ice-template) method, in which the porous structure is generated through the solidified solvent, the porous structure in the acquired 3D PCL scaffolds is formed upon the random self-agglomeration of shortened nanofibers. Such a porous structure is similar to that in natural extracellular matrixs (ECMs), thus the 3D scaffolds would be suitable for cell functions and tissue formation.

2.2.2. Dispersion medium

To make a uniform dispersion of short nanofibers and tiny pieces of PCL and to maintein good control of nanofiber self-agglomeration during the subsequent thermal treatment, gelatin aqueous solution was added into PCL ethanol suspension [33]. If ethanol alone was used as the medium, the viscosity of suspension system was too low, and there would not be enough physical resistance in the system during the thermal treatment; as a result, the agglomeration of PCL nanofibers would occur too fast, leading to very firm/dense agglomerate. Therefore, gelatin was chosen to increase the viscosity of suspension system due to its biological origin, biodegradability, biocompatibility, and commercial availability; while deionized (DI) water was also added for improving the solubility of gelatin in the mixture system. After the gelatin and DI water were added to the system, short nanofibers and tiny pieces of PCL were stabilized by gelatin molecules and could be uniformly dispersed. Although the samples were rinsed with DI water for several times, some gelatin was still remained on the surface of nanofibers, making the nanofibers and the resulting 3D structures hydrophilic.

2.2.3. Binding agent

Instead of using additional binding agents, PCL itself works as a binder during the TISA process. PCL is a cost-effective, biocompatible, biodegradable, and FDA-approved polymer. Due to low degradation rate, PCL can act as a steady binder to stablize the 3D structure in a long tissue regeneration period. PCL also has good spinnability and the ability to blend with various polymers. Besides, owing to the low glass-transition temperature (−60 °C) and melting temperature (60 °C), PCL possesses good mechanical property/elasticity. Upon submerging the shortened PCL nanofibers into a water bath at 55 °C, the nanofibers gradually self-agglomerate and form a stable 3D nanofibrous structure with interconnected and hierarchical pores. In principle, the TISA method could be applied to various polymer nanofibers, as long as the heat treatment temperature is close to their melting point. However, the melting temperatures of most polymers are very high (over 160 °C), and the high boiling point solvents are needed to partially melt/soften the nanofibers. Nevertheless, these solvents are usually hard to be removed completely and the residual solvent may be toxic to cells. In addition, even if high boiling point solvents are used, shortened nanofibers can self-agglomerate together but cannot

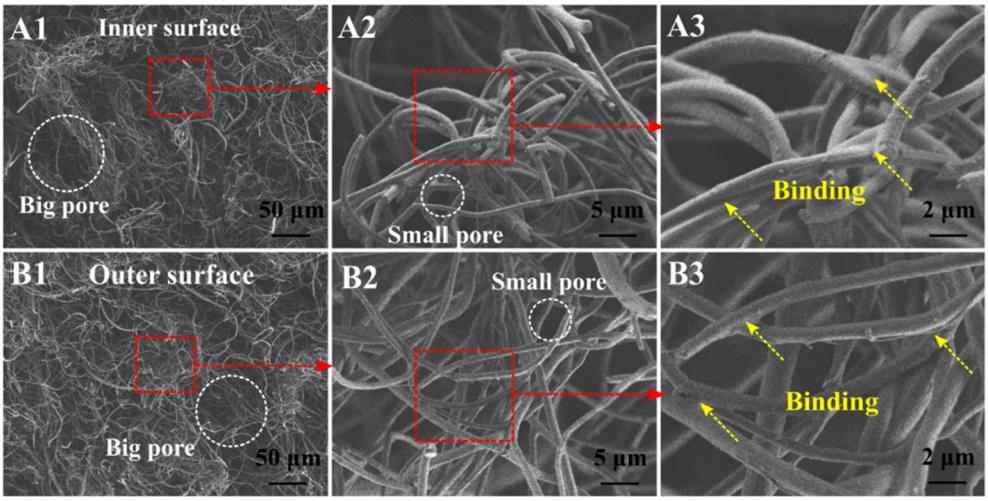

Fig. 8. SEM images showing typical morphologies of the inner surface (A1-A3) and outer surface (B1-B3) of electrospun CA/PCL scaffold. High magnification SEM images (A3) and (B3) showing the binding locations. Reproduced with permission from (2018) Elsevier [68].

remain stable structure because of their high stiffness/modulus. Hence, blending PCL with other polymers and using it as the binding agent to fabricate 3D scaffolds is a promising approach to solve the above problem thus to expand the application of TISA method.

To demonstrate the feasibility of using PCL as binding agent to develop 3D scaffolds, electrospun cellulose acetate (CA) scaffold with PCL as the biodegradable and biocompatible binding agent was successfully fabricated (Fig. 8) [68]. The CA/PCL (mass ratio: 75/25) 3D scaffold did not contain any toxic crosslinking agent. It is morphologically similar to natural ECM thus well suitable for cell functions and tissue formation. More importantly, all of the polymers which could be blended with PCL can be developed as 3D scaffolds by the TISA method followed by thermal stabilization, which might considerably expand the application of electrospun 3D scaffolds to various tissue engineering areas.

2.2.4. Modification and functionalization

In the field of tissue engineering, polymeric biomaterials which possess excellent overall properties/functions are highly desired, whereas no single available polymer can fulfil all the requirements. Therefore, blending two or more polymers could be a promising approach to fulfill these demands and to fabricate innovative and highly efficient biomaterials. Through combining adequet polymers and adjusting their weight ratio, electrospun blend nanofibrous scaffolds can be tailored to possess desired functions. For example, PCL has been widely used in tissue engineering but has limited cell affinity and/or bioactivity due to its hydrophobicity and lack of surface cell recognition sites; while blending biologically derived polymers or synthetic polymers with PCL can modulate the bioactivity, hydrophilicity, degradation rate, and mechanical properties. In our previous work, we modified PCL with more bioactive PLA and developed 3D PCL/PLA blend (weight ratio: 4/1) nanofibrous scaffolds *via* the TISA method [50]. The resulting scaffolds had high porosity (~95.8%) with interconnected and hierarchically structured pores having sizes ranging from sub-micrometers to ~300 μm. Compared to 3D PCL scaffolds, the 3D PCL/PLA blend scaffolds had higher mechanical properties and *in vitro* bioactivity. In a follow-up study, the electrospun nanofibrous scaffolds with different weight ratios of PCL/PLA (*i.e.*, 100/0, 60/40, and 20/80) were fabricated. With the PLA weight ratio increase in 3D PCL/PLA blend scaffolds, the osteogenic differentiation of human mesenchymal stem cells (hMSCs) was substantially enhanced [69]. To date, various biologically derived polymers (including proteins [70–72], polysaccharides [73,74], and polyhydroxyalkanoates [75–77]) and synthetic polymers (including polyesters [78–81], water-soluble polymers [82,83], and conductive polymers [84]) have been blended with PCL for making electrospun polymer blend nanofibers. It is envisioned that all of these polymers could be fabricated into 3D scaffolds by first making blend nanofibers with PCL followed by processing *via* the TISA method; hence, a variety of electrospun 3D nanofibrous scaffolds would be available for various tissue engineering applications.

PCL and PCL blends could barely meet the requirements for being tissue engineering materials, whereas they are not sufficient to fully mimic the biological properties of ECM. Functional fillers are able to provide the scaffold with more features that the biomaterials themselves do not possess, which could better mimic natural ECM. For example, bioactive inorganics could mimic the natural bone component. Carbon materials render the scaffolds with conductive feature, which would provide electrical stimulation to cardiac, muscle, and nerve tissues to mimic the electrical signal in the human body. To date, different functional fillers such as bioactive inorganics [85–87], carbon nanomaterials [88,89], polysaccharides [90,91], nanoclay [92], and metal/metallic oxides [93–95], have been incorporated into electrospun PCL nanofibers; and these fillers might be able to functionalize electrospun 3D PCL scaffolds.

Cells interact with scaffolds primarily through the surface of scaffold materials, which can be controlled/tailored upon adjusting the surface chemical properties. Besides incorporating functional fillers directly into the scaffold nanofibers, surface modification is another effective approach to generate chemical specificity and recognition, which can lead to desired specific intracellular signaling. In our group, to further improve the scaffold's bioactivity and promote new bone formation, we functionalized 3D PCL scaffolds with

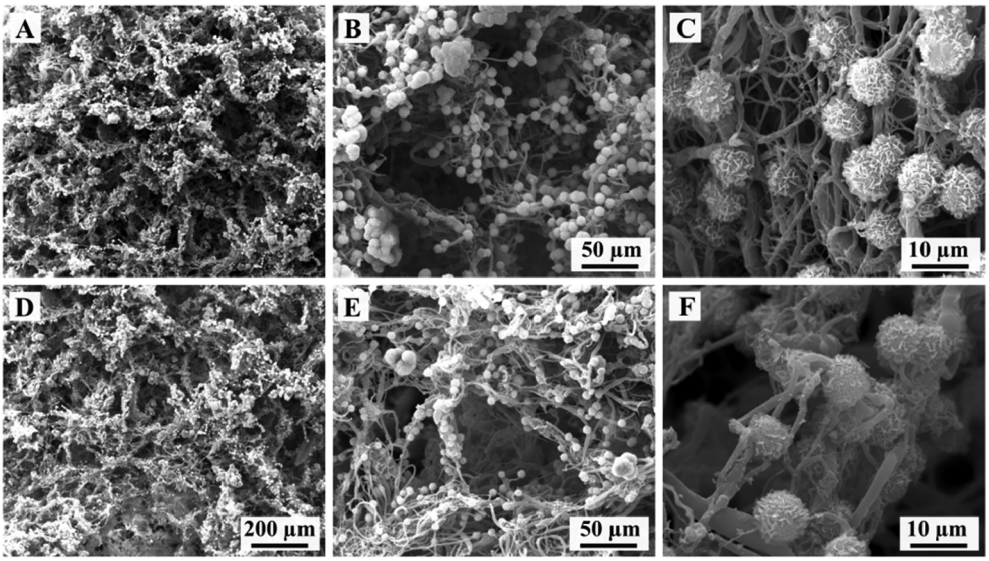

Fig. 9. SEM images showing the representative morphologies of external surface (A–C) and internal section (D–F) of PCL scaffolds coated with HA. Reproduced with permission from (2017) Elsevier [96].

hydroxyapatite (HA) (Fig. 9) and BMP2 signaling activator phenamil, which provided a favorable osteogenic niche for bone formation at low doses of BMP2 [96]. We believe that several other surface modification methods on electrospun PCL nanofibers including surface activation [97,98], chemical grafting [99–101], copolymerization [102–105], and biomimetic modification [106–111] could also be adopted to modify the electrospun 3D PCL scaffolds.

3. Properties of 3D monolithic structures assembled from fragmented electrospun nanofiber mats/membranes

3.1. Density and porosity

3D structures assembled from fragmented electrospun nanofiber mats/membranes usually possess ultralow density and extremely high porosity, which can be tuned by controlling the amount of nanofibers. The ultralight feature (*i.e.*, density below 10 mg cm^{-3}) could be readily achieved in most electrospun 3D structures. Further modification of 3D structures such as incorporation of nanoparticles [62] or nanofiber surface coating [67] would result in the increase of density (up to tens of mg cm^{-3}). To date, the lightest electrospun 3D structure with the density of 0.12 mg cm^{-3} and porosity of 99.992% was obtained by Ding's group [31]. As illustrated in Fig. 10, the isotropically bonded elastic reconstructed nanofibrous aerogels (*i.e.*, FIBER NFAs) with density of 0.12 mg cm^{-3} can easily stand on the tip of feather and even float on cold air.

The density and porosity have direct impacts on mechanical properties. The porous structure is also responsible for many unique

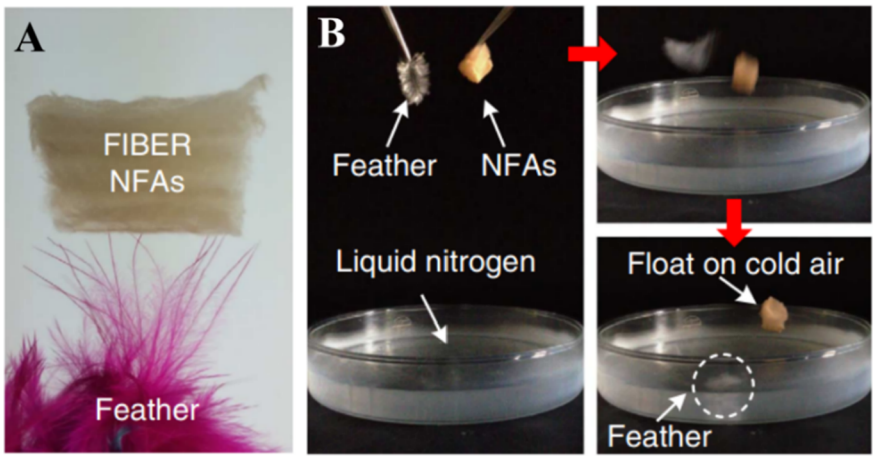

Fig. 10. (A) An electrospun aerogel/sponge (ρ = 0.12 mg cm^{-3}) stands on the tip of dyed feathers. (B) Photographs demonstrating that the ultralight aerogel can float on cold air. Reproduced with permission from (2014) Nature Publishing Group [31].

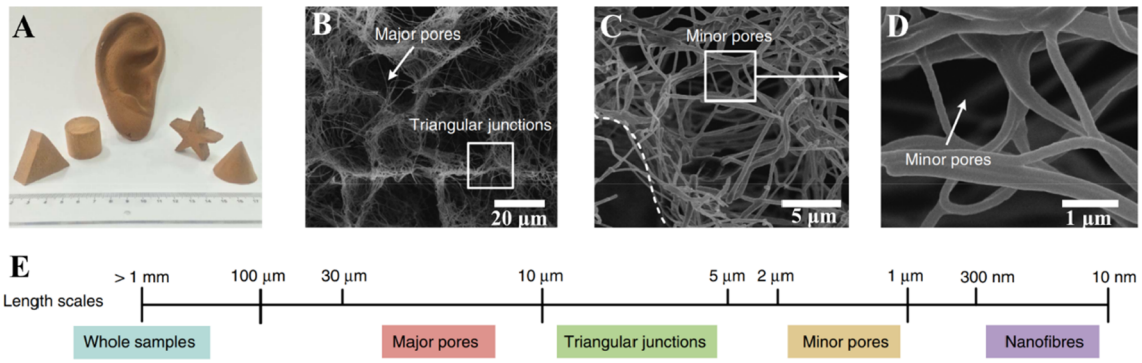

Fig. 11. (A) Photograph of FIBER NFAs with various shapes. (B–D) The microscopic architecture of FIBER NFAs at different magnifications, showing the hierarchical cellular fibrous structure. (E) Schematic representation of the dimensions of relevant structures. Reproduced with permission from (2014) Nature Publishing Group [31].

properties, resulting in various applications. For example, the excellent thermal insulation of PI sponge [47] could be attributed to the high porosity of 3D structure/sponge filled with air. In PAN/PI/CNFs sponge based pressure sensor [46], the response of resistance change under compression strain is contributed by the hierarchical porous structure; in specific, the large pores lead to large deformation, wide strain range, large resistance change, and high sensitivity. Low density and high porosity lead to high absorption capacity [49]. In tissue engineering area, high porosity provides more space/volume for cell growth [33].

3.2. Morphology and pore structures

Owing to simplicity of the assembly process and the facile availability of electrospun nanofibers, the shapes of 3D structures can be controlled and the fabrication is possible to be scaled up. As illustrated in Fig. 11A, integrated FIBER NFAs with desired shapes were readily prepared and the FIBER NFAs can be easily scaled up by simply using a large shaping mold. During the freeze drying process, the dispersed nanofibers were enriched and entrapped among the solvent crystals. The structure of 3D architecture was a replica of that of the solidified solvent, and the size distribution of large pores was determined by the size of solvent crystals. The assembly of shortened electrospun nanofibers, on the other hand, resulted in small pores. Different magnificaton SEM images in Fig. 11B–D were acquired from a typical FIBER NFAs with the density of 9.6 mg cm^{-3}. The cellular architecture showed an open-cell architecture with major cellular pores (10–30 μm) and these cells were interconnected with each other by triangular junctions (Fig. 11B), which consisted of numerous minor cellular pores with sizes of 1–2 μm (Fig. 11C & D). The dimensions of relevant structures were shown in Fig. 11E.

The large pores can be tuned by controlling the freezing rate. In our group, we investigated the effects of freezing rate to pore structures [46]. During the freezing process, fast cooling rate would lead to rapid homogenous nucleation process that could generate many nuclei; and small crystals were then grown in the sample. As a result, the 3D structure/sponge formed by fast freezing had small pores (< 2 μm) and narrow pore size distribution, whereas the 3D sponge formed by slow freezing had hierarchical pores combining large pores (~100 μm) and small pores (< 2 μm). Adlhart's group [112] also studied the effect of freezing conditions on these structures and found the similar results. By increasing the freezing-front velocity from 2 to 200 μm s^{-1}, the pore size was decreased from 123 to 9.5 μm (Fig. 12).

3.3. Surface wettability

The surface wettability of electrospun 3D structures could be adjusted through surface modification. For example, the hydrophilic surface could be achieved by coating gelatin on hydrophobic PCL [33] and PCL/PLA scaffolds [50]; note that high hydrophilicity of a scaffold is crucial for the tissue engineering application. On the other hand, superhydrophobicity could be obtained through surface modifications such as incorporation of SiO_2 nanoparticles (Fig. 13A) [62], PPX CVD coating (Fig. 13B) [67], and silane CVD coating (Fig. 13C) [113]. In our group, thermal stabilization at 230 °C was applied to convert electrospun 3D cellulose sponge from hydrophilic to hydrophobic (Fig. 13D) [49]; and these hydrophobic/superhydrophobic 3D structures demonstrated excellent capability for the absorption of organic solvent/oil. It is noteworthy that the chemical modifications often require precisely controlled conditions and expensive chemicals, while the thermal stabilization is an cost-effective approach for surface modification.

3.4. Specific surface area

The reported 3D structures generally have low BET specific surface areas, primarily due to lack of porous structures within nanofibers. For example, Duan *et al.* reported the specific surface area of 2.66 m^2 g^{-1} for a sponge with density of 3.75 mg cm^{-3} [32]. The BET specific surface area can be increased through chemical threatments of nanofibers. For example, Kim and co-workers [114] reported a microporous organic polymer sponge with core-shell structure (PVASi@TEDB-NH_2), which was fabricated *via*

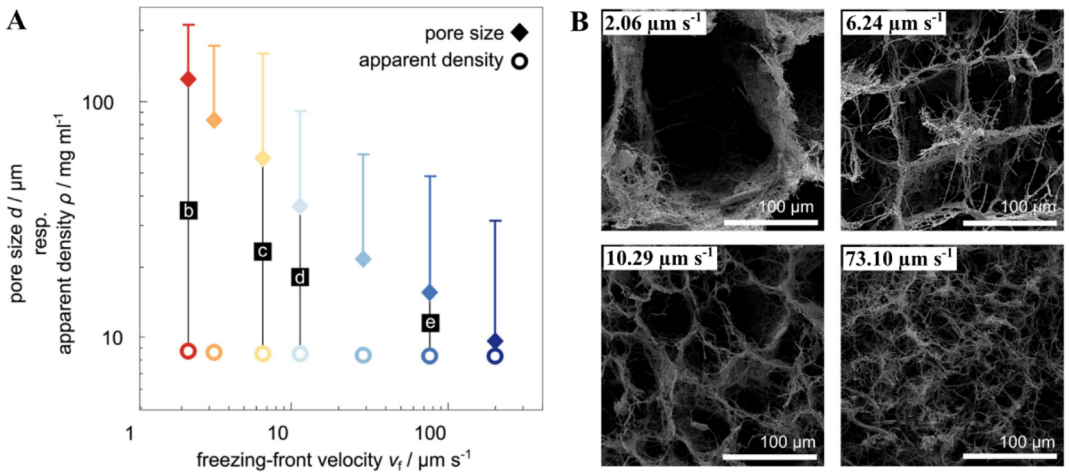

Fig. 12. (A) Effect of freezing conditions on sponge microstructure. Slow freezing-front velocities provide the largest pore diameters, while the sponges' apparent density remained constant within 8.7 ± 0.1 mg mL^{-1}. (B) SEM images show cross-sections of respective sponges at the center height of 7.5 mm obtained with different v_f. Reproduced with permission from (2016) Wiley [112].

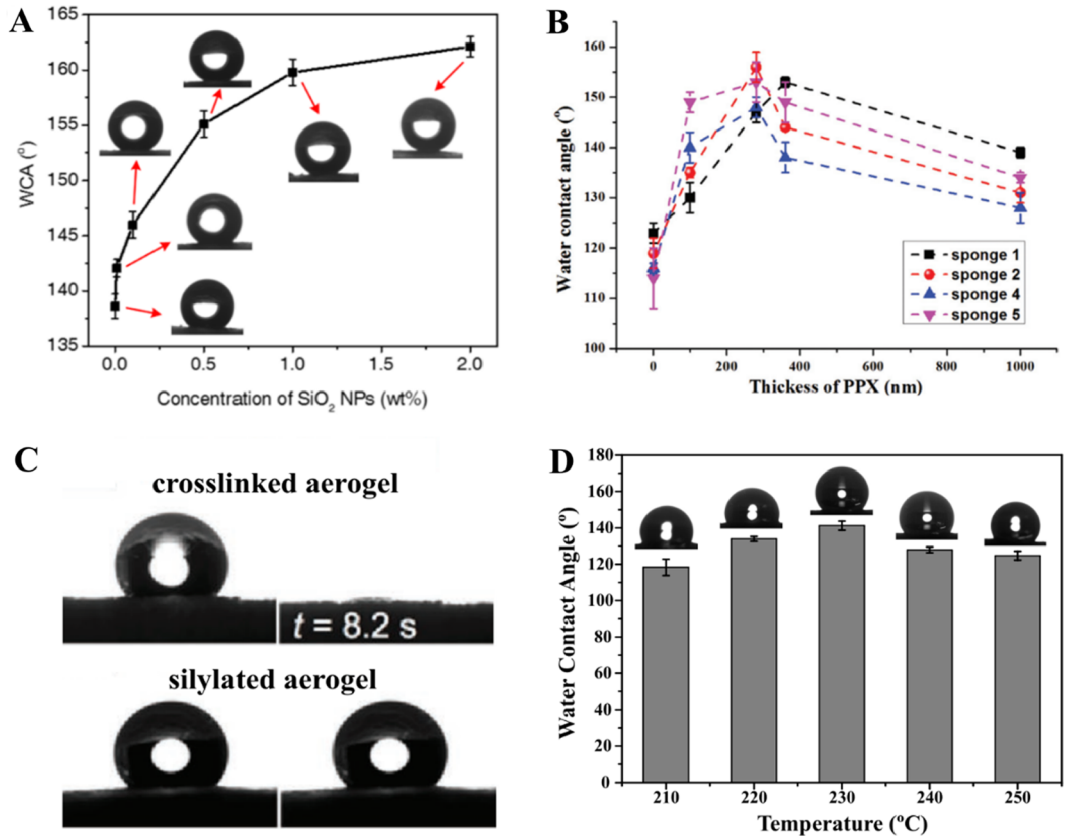

Fig. 13. (A) Water contact angle of the FIBER aerogels/sponge with increasing SiO_2 NPs concentrations. Reproduced with permission from (2015) ACS [62]. (B) Water contact angle as a function of the PPX coating thickness of sponges 1, 2, 4, and 5. Reproduced with permission from (2016) RSC [67]. (C) Water contact angle of the amphiphilic cross-linked pullulan/PVA aerogel and the hydrophobic silylated aerogel. Reproduced with permission from (2017) Wiley [113]. (D) Water contact angle of ultralight electrospun cellulose sponge stabilized under different temperatures. Reproduced with permission from (2018) Elsevier [49].

Sonogashira-Hagihara coupling reaction of 2,5-dibromoaniline and 1,3,5-triethynylbenzene (TEDB) in a uniform suspension of PVASi nanofibers. The modified sponge displayed a combination of type I and IV isotherms, indicating the existence of micropores and mesopores. Such PVASi@TEDB-NH_2 sponges exhibited an average BET specific surface area of 447 $m^2\ g^{-1}$. In general, chemical (*e.g.*,

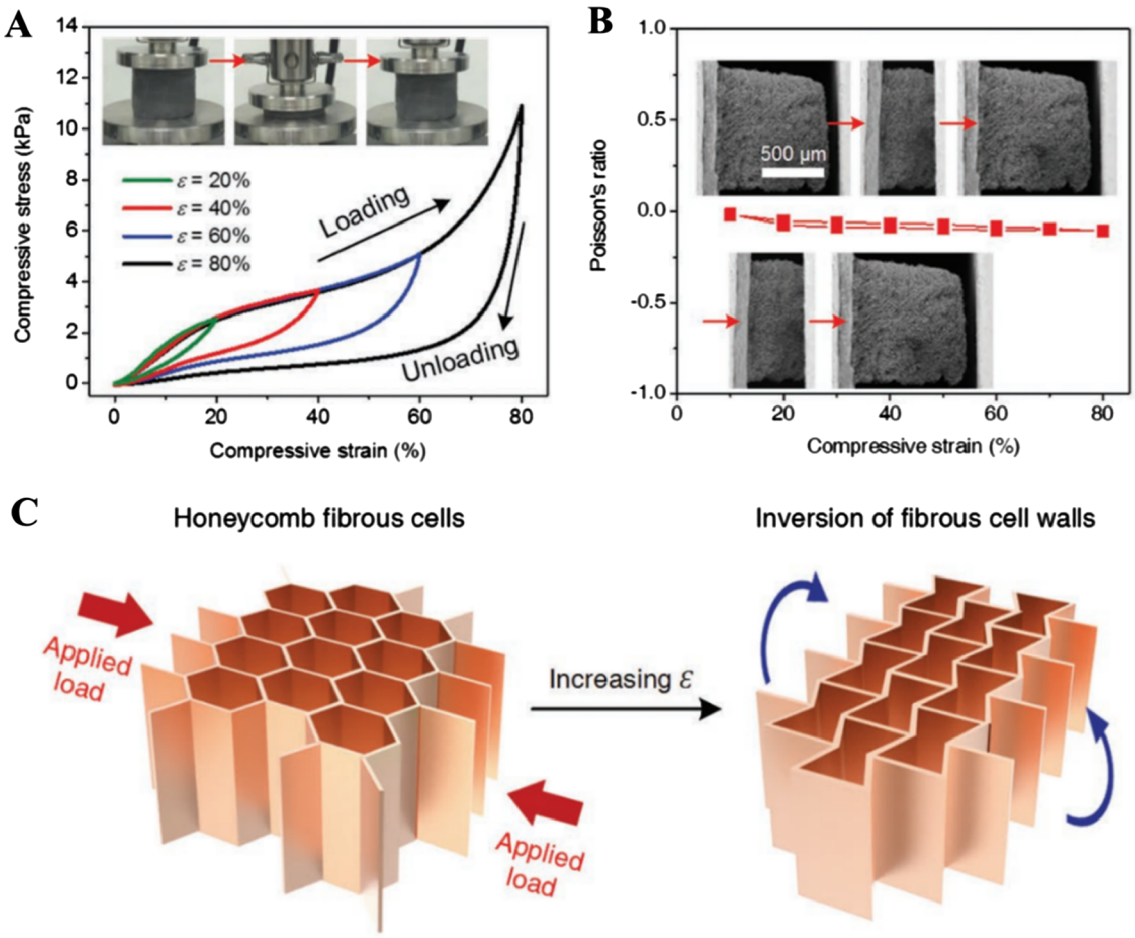

Fig. 14. (A) Compressive stress (σ) *vs.* compressive strain (ε) curves for CNFAs along the loading direction. Insets showing the profiles of the CNFAs during a compressing cycle (ε = 80%). (B) The Poisson's ratio of the CNFAs as a function of increasing compressive strain to 80%. Inset: SEM observations of the CNFAs under cycled compression and release, focusing on a small piece (< 1 mm). (C) Schematic representation showing the inversion of nanofibrous cell walls with compressive strain. Reproduced with permission from (2016) Wiley. [52]

using reagents such as NaOH, KOH, and H_3PO_4), thermal (*e.g.*, through carbonization of electrospun blends including polymer and inorganic salts), and other (*e.g.*, using oxidizing gases, plasma treatment, and acid corrosion) treatments could be applied to activate electrospun nanofibers and to acquire micropores and mesopores, and the resulting structurs/sponges might be highly desired for supercapacitor and/or adsorption applications.

3.5. Mechanical properties

Even though electrospun nanofibers are soft/weak, the resulting 3D monolithic porous structures could be mechanically robust; this is due to the support of flexible nanofibers, durable nanofiber binding, and porous structure. Elastic nanofibers such as SiO_2 and PI are usually applied to improve the integrity and elasticity of 3D structures. For example, Si *et al.* [52] developed super-elastic carbonaceous nanofibrous aerogels (CNFAs) with an ordered honeycomb-like structure using konjac glucomannan and flexible SiO_2 nanofibers. The CNFAs exhibited robust mechanical properties, and the structure could endure large compressive deformations without cracks, similar to honeycomb-structured materials. As shown in Fig. 14A, three obvious regions including an elastic linear region ($\varepsilon < 20\%$), a plateau region ($20\% < \varepsilon < 60\%$), and a densification region ($\varepsilon > 60\%$) were observed; additionally, these CNFAs had the Poisson's ratio close to zero when compressed in one direction (Fig. 14B), owing to the inversion of the nanofibrous cell wall (Fig. 14C). Furthermore, the CNFAs exhibited relatively minor plastic deformations (~4.3%) after 1000 compressive cycles at the 50% strain.

PI nanofibers were selected for providing the elasticity to PAN/PI/CNFs sponge in our group [46]. The resulting conductive sponge was mechanically robust and possessed superior stability when being used as a compressive strain sensor. Jiang *et al.* [47] also reported a neat PI nanofiber sponge, which showed excellent compressive strength and super flexibility after being compressed for 10,000 times. However, these reported 3D structures/sponges only had excellent mechanical properties under compression strain;

while their performances under the tensile/stretching strain are upon further improvement. The thermally induced intermolecular condensation (at 500 °C) has recently been applied to make electrospun PI nanofiber aerogel (PINFAs), and the resulting aerogel could be stretched with the elongation and stress at break values being 11.5% and 13 kPa, respectively [60]. The excellent mechanical performance can be attributed to rigid macromolecular chain, as well as physical entanglements and chemical crosslinkings among the nanofibers.

It is important to note that electrospun nanofibers are the main component in the 3D structures/sponges/aerogels/scaffolds discussed in this review. Besides, shortened nanofibers can also be added into traditional aerogels/sponges, acting as the reinforcing fillers (rather than the main component) [115–118]. For example, PAN nanofibers and GO nanosheets have been incorporated into resorcinol-formaldehyde to produce 3D aerogels with high structural stability and strength [116]; and cellulose acetate nanofibers have been added in GO aerogels to prevent the GO sheets from over-stacking and to improve the connectivity of cell walls [117]. Intriguingly, the PI aerogel could be reinforced by using PI nanofibers as the fillers [118]; the short PI nanofibers improved the strength/toughness of PI aerogel by dissipating the applied stress along the pore walls and nanofibers *via* mechanical interlocking effect, leading to a 2-fold improvement on compressive modulus than neat PI aerogel.

3.6. Electrical properties

Conductive 3D structures can be prepared by using precursor nanofibers as building blocks (followed by carbonization) or by mixing with conductive component/filler. For example, synthetic polymers such as PAN and PI, or biomass such as konjac glucomannan (KGM) are commonly used precursors to fabricate carbonaceous materials; 3D carbonaceous aerogels/sponges assembled from PAN/SiO_2 [31], SiO_2/KGM [52], PAN/PI [45], and PAN/GO [54] have been prepared and studied for pressure sensing and energy storage.

However, the electrical conductivity of these carbon structures is determined upon the carbonization process and is difficult to be precisely controlled/adjusted. Recently, our group has reported a general approach to prepare the mechanically robust 3D nanofibrous sponge with tunable conductivity [46]. The key is to use carbonized nanofibers and other polymer nanofibers as the building blocks for the preparation of 3D conductive sponge. The sponge contains short electrospun carbon nanofibers (ECNFs), which act as the conductive component and are randomly mixed with electrospun PAN and PI nanofibers. By adjusting the amount of ECNFs, the conductivity of the 3D sponge can be precisely tailored, as shown in Fig. 15. The prepared 3D sponge is an ideal candidate for highly sensitive pressure sensor. In another study, Jiang *et al.* [119] investigated the electrical conductivity of porous sponge containing a double network of Ag nanowires and PI. The stress-responsive and highly flexible sponge showed the electric conductivity from 170 to 16660 S m^{-1} depending on the applied stress, and the sponge could be used for the fabrication of efficient Joule heater.

3.7. Thermal properties

The thermal properties of 3D structures are determined by the properties of electrospun nanofibers. For example, SiO_2 nanofibers were used to prevent the volume shrinkage during thermal treatment [31,62]; they could also serve as the matrix in high-temperature carbon aerogel [52], and could be used to make fire-resistant ceramic nanofibrous aerogel [120]. Recently, Jiang *et al.* [47] have developed thermally insulating elastic sponges by using PI as high-temperature stable polymer. The sponges exhibited initial degradation above 400 °C and 500 °C in air and nitrogen, respectively (Fig. 16A). Compared to the SG and SGPPX samples (polyacrylate based sponges without and with PPX coating, respectively), PISG-50 (PI sponge with the density of 10.1 mg cm^{-3}) remained stable under 300 °C for 0.5 h (Fig. 16B). The PI sponge (PISG-50) exhibited the low thermal conductivity of 0.026 W mK^{-1} (similar to air) without compression, which was due to the high specific pore volume (98.3 cm^3 g^{-1}) of the sponge. In the compressed status, the thermal conductivity of PISG-50 slightly increased and the thermal diffusivity decreased. Si *et al.* [120] fabricated super-elastic lamellar-structured ceramic nanofibrous aerogels (CNFAs) through combination of electrospun SiO_2 nanofibers with aluminoborosilicate matrices. The CNFAs with the density of 10 mg cm^{-3} showed a low thermal conductivity of 0.025 W mK^{-1}, which was very close to that of air under ambient conditions (0.023 W mK^{-1}). When the density of the CNFAs decreased to 0.5 mg cm^{-3}, the thermal

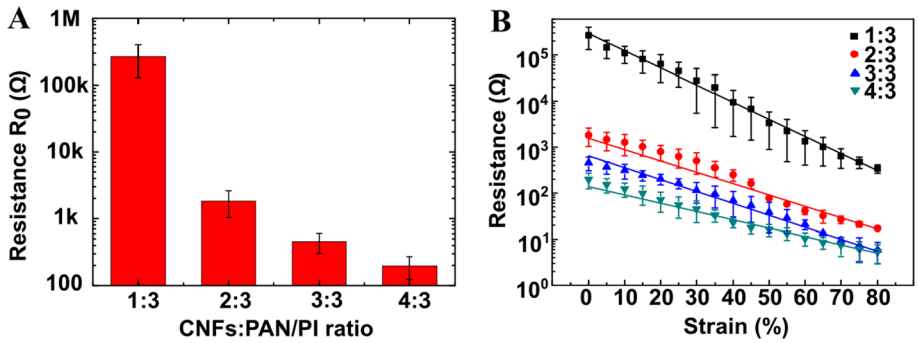

Fig. 15. (A) Resistance values of 3D conductive sponges with different CNFs to PAN/PI ratios. (B) Resistance variations of the 3D conductive sponges under different compressive strains. Reproduced with permission from (2017) RSC [46].

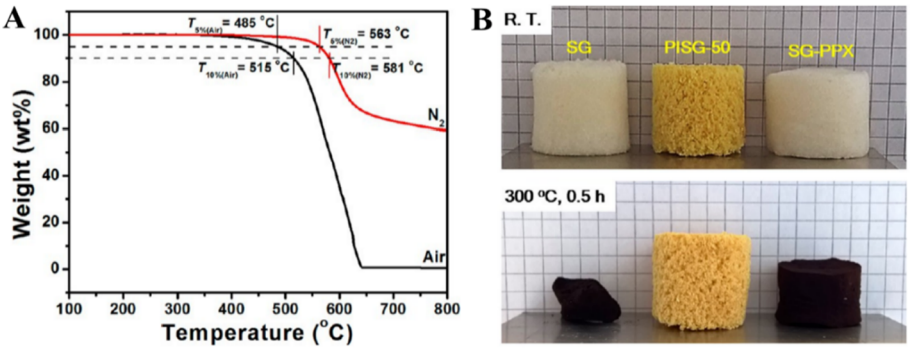

Fig. 16. (A) TGA curves of PI sponge (sample PISG-50). (B) Photographs showing thermal resistance of sponges SG, PISG-50, and SG-PPX at room temperature (Top) and 300 °C (Bottom) for 0.5 h. Reproduced with permission from (2017) ACS [47].

conductivity slightly increased to 0.032 W mK^{-1} due to the increase of pore size.

3.8. Biocompatibility and biodegradability

For the application of 3D structures in tissue engineering and drug delivery, the nanofibers used to make these structures need to be biocompatible and biodegradable. To date, PCL [33], PCL/PLA [50], gelatin/PLA [121], poly(L-lactic acid-co-ε-caprolactone)/silk fibroin [122], and PLGA/collagen/gelatin [123] have been reported to fabricate 3D tissue engineering scaffolds. For example, the cell viabilities of hMSCs on electrospun PCL-3D and PCL/PLA-3D scaffolds were quantitatively measured by MTS assay after culturing for 1 and 3 days [50]. As shown in Fig. 17A, both scaffolds exhibited similar cell viabilities after 1 day of culture; on day 3, the cell viability on PCL/PLA-3D scaffolds was moderately but significantly higher than that on PCL-3D scaffolds ($P < 0.05$). In addition to cell viabilities, hMSCs morphologies on PCL-3D and PCL/PLA-3D scaffolds were investigated after culturing for 16 h. As shown in Fig. 17B1 and B2, cells adhered and spread well with a typical fibroblastic morphology on both types of scaffolds, indicating the good biocompatibility.

4. Applications of 3D monolithic porous structures assembled from fragmented electrospun nanofiber mats/membranes

4.1. Environment

4.1.1. Organic compound removal

3D absorbent materials with superior capacity for selective absorption/removal of organic compounds (*e.g.*, oils and organic solvents) are urgently needed to resolve the oil spillage and industry organic solvent discharge [124–127]. Electrospun 3D nanofibrous structures have been explored as innovative materials for the absorption of organic compounds. For example, SiO_2 nanoparticles were incorporated into 3D electrospun PAN nanofibrous aerogels; and the resulting 3D PAN/SiO_2 hybrid aerogels showed superhydrophobic/superoleophilic feature, which could effectively separate surfactant-stabilized oil droplets from an aqueous emulsion with high flux value (up to 8140 ± 220 $L{\cdot}m^{-2}{\cdot}h^{-1}$) and excellent separation efficiency [62]. Another exampe, Deuber and co-workers [113] developed hierarchically structured and ultralight pullulan/PVA aerogels, in which silane coating was used to convert the hydrophilic aerogel to be hydrophobic; the resulting sponge allowed the selective separation of organic liquids based on

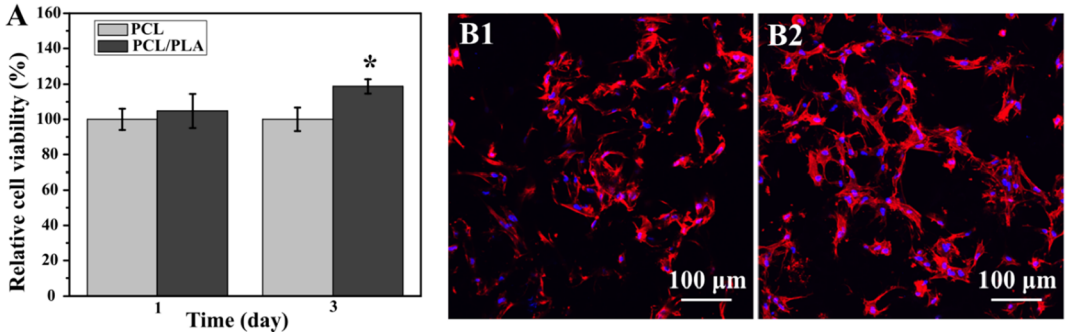

Fig. 17. (A) hMSCs viabilities on PCL-3D and PCL/PLA-3D scaffolds after culturing for 1 and 3 days. hMSCs morphologies on (B1) PCL-3D and (B2) PCL/PLA-3D scaffolds after culturing for 16 h. Note that PCL-3D scaffolds are included as control samples. Data are expressed as mean ± SD (n = 3). Fluorescence micrographs of chondrocytes seeded on 3DS-2 (modified gelatin/PLA scaffold crosslinked with hyaluronic acid (HA)) for 7 days. Live and dead cells dyed green and red, respectively. Reproduced with permission from (2017) Elsevier [50].

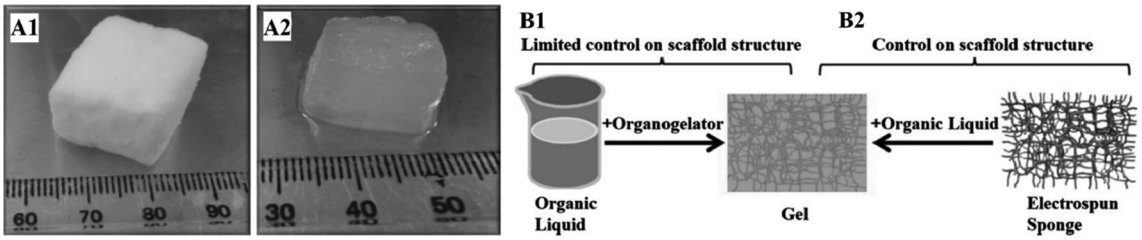

Fig. 18. A sponge made of electrospun fibers with the mass of 0.03 g (A1) and the sponge after uptaking 30 g of mineral oil (A2). A schematic showing the formation of organogels by the action of organogelators on liquids (B1) and by soaking electrospun fiber sponges with liquids (B2). Reproduced with permission from (2017) Wiley [129].

their different relative dielectric constants. In 2017, Lu *et al.* [128] reported the direct fabrication of highly hydrophobic (*i.e.*, superoleophilic) and chemically crosslinked poly(vinyl alcohol-*co*-ethylene) (EVOH) nanofiber aerogels without any hydrophobic modification. The obtained crosslinked EVOH aerogels showed excellent absorption capacity values (ranging from 45 to 102 times of their own weights) to various oils and organic solvents.

As first reported by Greiner and co-workers [67], poly(p-xylylene) could be utilized to modify ultralight electrospun sponges through chemical vapor deposition; and the resulting sponges showed substantial improvements on compression strength, water contact angle, and solvent resistance. Interestingly, upon absorption of organic solvents, these sponges could be turned into mechanically stable gel-like materials (*i.e.*, spongy gels) (Fig. 18A1 & A2) [129]. The appearance of such spongy gels is similar to classic organogels. Typically, organogels are formed by a bottom-up process (Fig. 18B1); while the spongy gels are formed through a top-down approach (Fig. 18B2), providing various advantages for the properties, reproducibility, and stability.

Although these 3D aerogels/sponges exhibited promising capability to absorb organic compounds, the usages of expensive modifying agents, organic solvents, and complicated processes are the major limitations; additionally, all of the above-described electrospun 3D nanofibrous structures were made from synthetic polymers derived from non-renewable petroleum resources. Recently, our group has made ultralight electrospun cellulose sponge (UECS) from regenerated cellulose nanofiber mat/membrane *via* freeze drying and thermal stabilization [49]. Compared to chemical modifications, which often require the precisely controlled conditions and expensive chemicals, thermal stabilization at 230 °C provides a substantially more convenient and cost-effective approach to convert cellulose from hydrophilic to hydrophobic, thus making cellulose available for more applications. The prepared UECS demonstrated superior absorption capacity (Fig. 19A) to organic compounds due to high porosity (99.57%), low density (6.45 mg cm^{-3}), and desired surface hydrophobicity (with water contact angle of ~141.2°). Furthermore, upon absorption of an organic compound, the morphologically stable UECS organic gel could be acquired. Therefore, the developed UECS might be a promising type of environmental friendly 3D nanofibrous materials for high-performance adsorption/separation of organic compounds from aqueous systems (Fig. 19B & C); and the resulting UECS absorbed with organic compounds could be utilized for various applications related to organic gels.

4.1.2. Dye adsorption

Synthetic dyes are widely used in various fields, while their discharge into environment leads to severe problems. Dye adsorption treatment has been proven to be an effective method because of simple process and low energy consumption [130]. Kim *et al.* [114] developed a microporous organic polymer nanofiber sponge (PVASi@TEDB-NH_2) with the average BET surface area of 447 $m^2\ g^{-1}$. When the PVASi@TEDB-NH_2 was compressed and released in an aqueous methylene blue (MB) solution, the dye adsorption occurred

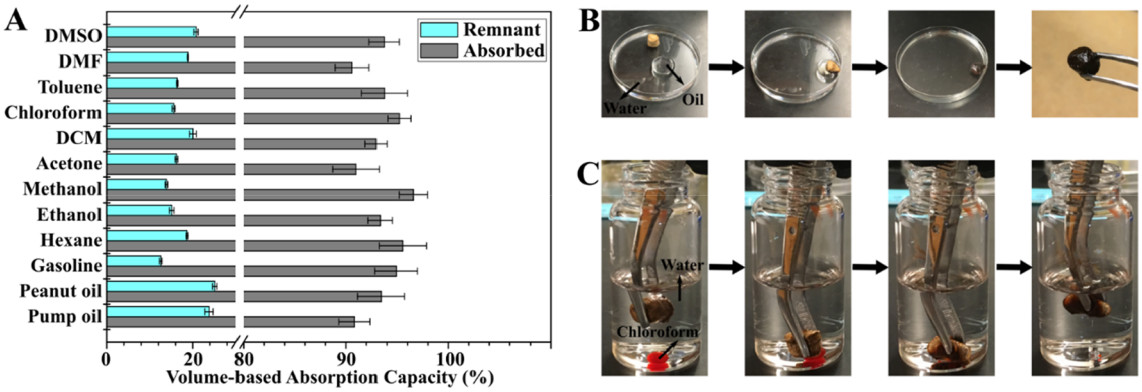

Fig. 19. (A) volume-based absorption capacities of UECS on different organic compounds. Photographs showing the separation performance of UECS on organic compounds. (B) Removing pump oil from the surface of water. (C) Collecting chloroform (containing the dye of Sudan I) from the bottom of water. Reproduced with permission from (2018) Elsevier [49].

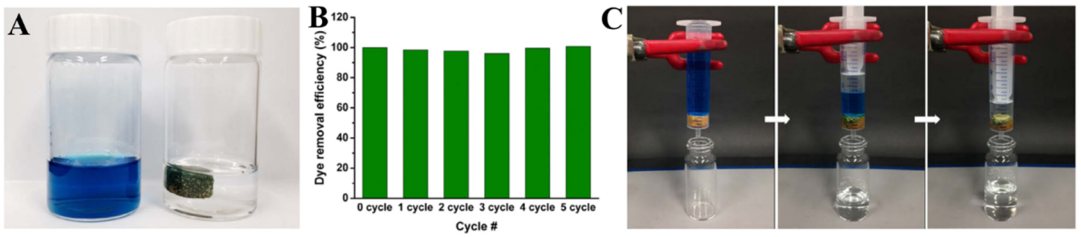

Fig. 20. (A) Photograph showing aqueous MB solutions before (left) and after (right) adsorption. (B) Results of PVASi@TEDB-NH_2 for MB adsorption by the compression and release process. (C) Sequential photographs showing the filtration process using the PVASi@TEDB-NH_2 syringe filter. Reproduced with permission from (2017) Elsevier [114].

rapidly (Fig. 20A). In addition, the dye adsorbed PVASi@TEDB-NH_2 could be reused upon simple regeneration through the Soxhlet extraction with methanol (Fig. 20B). PVASi@TEDB-NH_2 could also be used as syringe filter because of its monolithic and compressible characteristics. As shown in Fig. 20C, PVASi@TEDB-NH_2 was fit into a syringe and the blue MB solution turned colorless after filtration. Mousavi *et al.* [131] developed ultralight and robust 3D nanofiber sponges from shortened pullulan/PVA/polyacrylic acid nanofibers. Their results demonstrated that these 3D sponges were promising adsorbents for cationic dyes owing to high adsorption capacity (~383 mg g^{-1}) and reusability, and the adsorption process could be defined by the Langmuir isotherm model. It was intriguing that the dye adsorption by 3D sponges was 4 times faster than that by as-electrospun nanofiber mat/membrane. When used in a continuous process as the deep-bed filter, the pressure drop through the 3D sponge was reduced by a factor of 40 while maintaining equal adsorption performance as for the nanofiber membrane.

Functionalized electrospun nanofibers have also been demonstrated as highly efficient, environmentally friendly, and cost-effective adsorbents for rear earth elements [132,133]. For example, Wang *et al.* [134] developed water-rich and super-elastic 3D nanofiber hydrogels from electrospun sodium alginate/polyacrylamide nanofibers *via* freeze-drying followed by chemical cross-linking with pyromellitic dianhydride. The prepared 3D nanofiber hydrogels with abundant carboxyl groups exhibited superior adsorption capacity for lanthanide ions (Ln^{3+}) and excellent reusability. Moreover, benefiting from the typical 4f transition luminescence feature, the resulting Ln^{3+} hydrogels possessed outstanding photo-luminescent property, suggesting great potentials for different applications (such as luminescent patterning and underwater fluorescent devices).

4.1.3. Filtration and separation

Particulate matter (PM) pollution has caused severe harmfulness to human health, and effectively removal of PM becomes a critical demand nowadays. Qian *et al.* [60] developed hierarchically structured porous polyimide nanofibrous aerogels (PINFAs) by utilizing electrospun PI nanofibers as building blocks. The aerogels possessed ultralow density, super-elasticity, high-temperature stability, low thermal conductivity, and excellent performance on $PM_{2.5}$ filtration. As shown in Fig. 21A & B, the filtration efficiencies of PINFAs, 3M 9001 particulate respirator, and electrospun PI nanofiber membranes (PINFMs) with the same area and mass were 99.9%, 71.1%, and 99.9%, respectively; whereas the pressure drop of PINFAs (177 Pa) was far below that of PINFMs (1460 Pa), due to the large differences in porosity. The long-term filtration efficiency of PINFAs was investigated by operating under the mass concentration of $PM_{2.5}$ above 200 μg m^{-3} for 22 h at the velocity of 0.25 m s^{-1}. The acquired filtration efficiency was above 99.9%, and the calculated sorption dynamics was approximately 4.3 μg g^{-1} s^{-1}. As shown in Fig. 21C & D, the hierarchically structured porous framework was well retained after long-term use; while a large number of particles were attached on the nanofibers. Because of high thermal stability, the PINFAs were suitable for filtration of high-temperature industrial gas and automobile exhaust.

In another study, Deuber *et al.* [135] explored the potential of ultralight nanofiber aerogels (NFAs) for particle/aerosol filtration. The NFAs had a tunable hierarchical cellular open pore structure, and high filtration efficiencies (up to 99.999%) at the most penetrating particle size. Upon tailoring the porosity of NFAs, the authors were able to adjust the number of permeated particles and the pressure drop. These NFAs acted as an innovative type of deep-bed filters, and they were capable of handling high dust loadings without any indication of performance loss or increase in the pressure drop. When the face velocity of air was increased from 0.75 to 6 cm s^{-1}, the filtration efficiency still remained high. Compared to commercial NFM particle filters, the NFAs had significant improvements on the pressure drop with the filtration time as well as the susceptibility against high face velocity of air.

The purification/separation of proteins are essential to biotechnology and pharmaceutical industries. Electrospun 3D nanofiber structures were developed for highly efficient and cost-effective purification/separation of proteins. For example, Fu and co-workers [136] developed the carboxylated monolithic aerogels consisting of flexible electrospun ceramic nanofibers that were surface-wrapped with functional polymers. Benefitting from these advantageous features such as unique cellular structure, outstanding underwater super-elasticity and compressive fatigue resistance, their ion-exchange nanofibrous aerogels (IENFAs) showed synchronously promoted static (2.9×10^3 mg g^{-1}) and dynamic (1.7×10^3 mg g^{-1}) lysozyme adsorption capacities and improved buffer flux (2.17×10^4 L $m^{-2}h^{-1}$, gravity driven), as well as outstanding performance stability and regenerability. Impressively, the IENFA-packed column was able to directly and continuously separate lysozyme from egg white solely driven by gravity (Fig. 22). In another study, the authors from the same group [137] developed phosphorylated nanofibrous aerogels (PNFAs) by combining electrospinning, cryogenically induced phase separation, and *in situ* phosphorylation modification for large-capacity and high-throughput protein separation. The preparation of such aerogels represents a new approach for the development of next-generation nanofibrous aerogel-based chromatographic media, which would be used for various bioseparation applications.

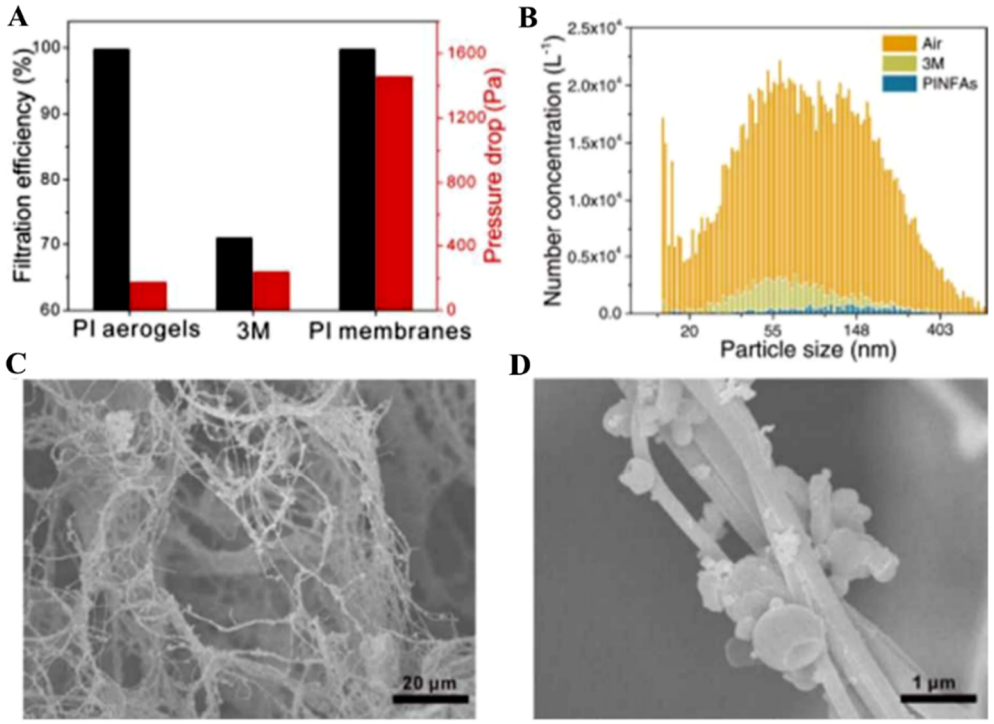

Fig. 21. Removal of $PM_{2.5}$ by PINFAs. (A) Conparison of filtration efficiency and pressure drop for PINFAs, 3 M, and PINFMs. (B) Number concentrations of $PM_{2.5}$ before and after filtration. Note that the number concentration of $PM_{2.5}$ after filtration by PINFMs was too low to be presented. (C & D) SEM images showing PINFAs after long-term filtration of $PM_{2.5}$. Reproduced with permission from (2017) RSC [60].

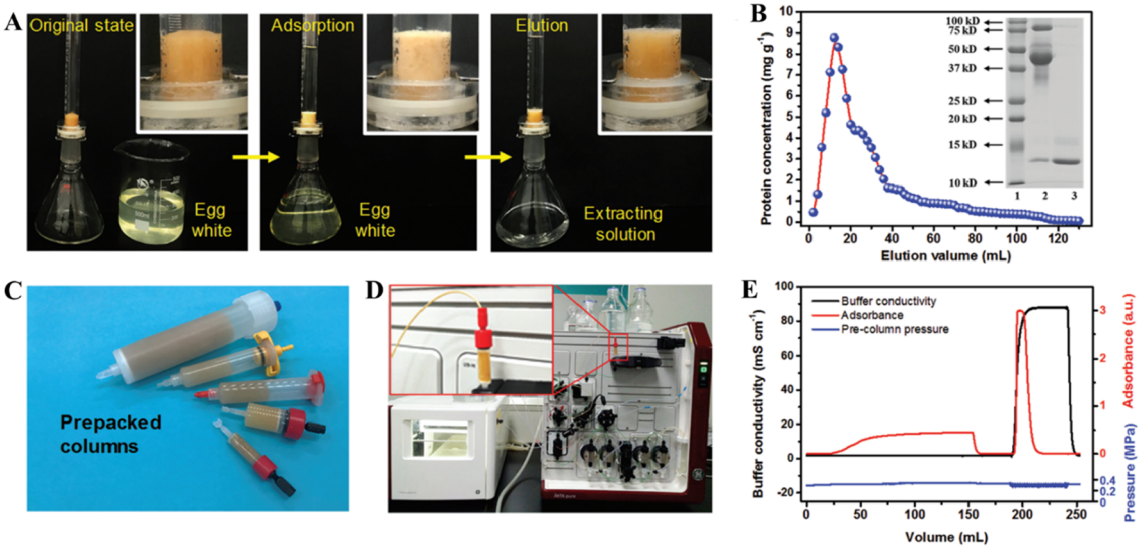

Fig. 22. (A) Photographs showing the continuous lysozyme separation and extraction by employing the IENFA-packed column. (B) Dynamic elution curves of the IENFA-packed column after extracted lysozyme form egg white. Insets displaying the corresponding SDS-polyacrylamide gel electrophoresis (PAGE) analysis of the obtained elution. (C) Various prepacked IENFA-flled chromatography columns. (D) Photographs showing the direct application of the IENFA-packed column on the ÄKTA pure 100 chromatographic system. (E) The obtained ÄKTA chromatogram of the 1 mL prepacked IENFAs' column at a processing rate of 150 mL h^{-1}. Reproduced with permission from (2019) Wiley [136].

4.2. Energy and electronics

4.2.1. Supercapacitor

Supercapacitors are important electrochemical energy storage devices. The capacitance of supercapacitors mainly comes from the

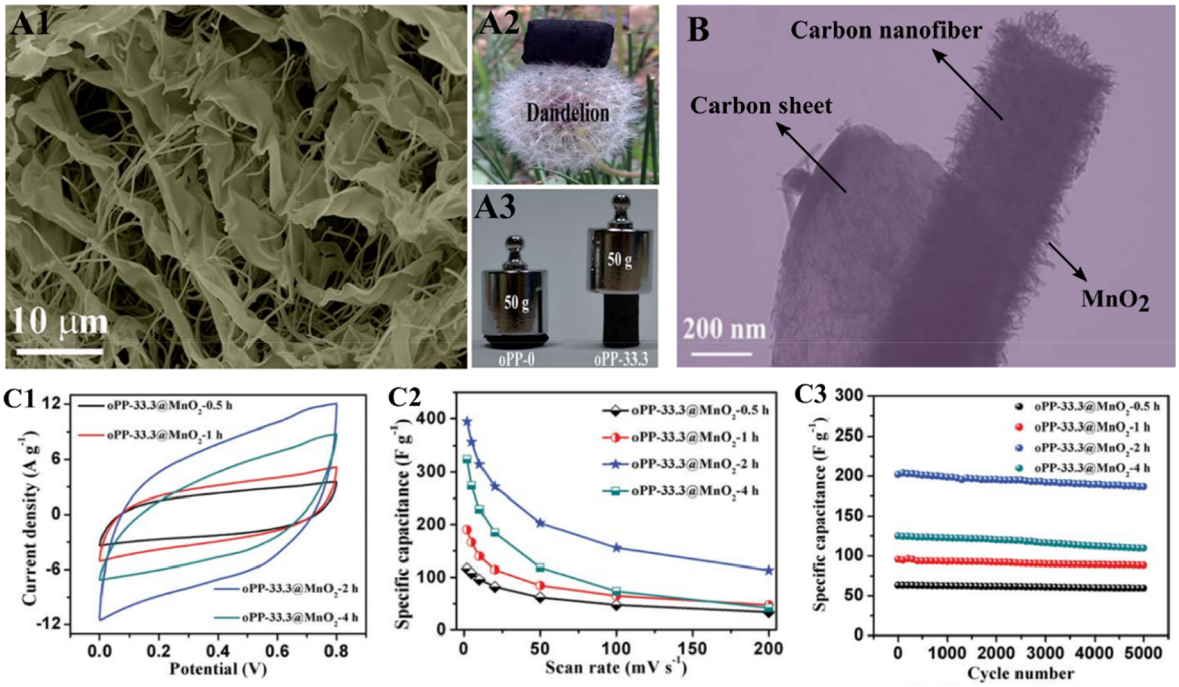

Fig. 23. (A1) A typical SEM image acquired from oPP-33.3 carbon aerogel, (A2) a photograph of oPP-33.3 carbon aerogel standing on a dandelion, and (A3) stress tolerance comparison between oPP-0 and oPP-33.3 carbon aerogels. (B) TEM image of oPP-33.3@MnO_2-2 h hybrid carbon aerogel. Electrochemical test results on the positive electrodes in an electrolyte of 1.0 M Na_2SO_4 using a three-electrode system: (C1) CV curves for oPP-33.3@MnO_2-x h hybrid carbon aerogels at the scan rate of 50 mV s^{-1} (where × = 0.5, 1, 2, and 4, respectively); (C2) rate stability of oPP-33.3@MnO_2-x h hybrid carbon aerogels at various scan rates; (C3) cycling stability of oPP-33.3@MnO_2-x h hybrid carbon aerogels at the scan rate of 50 mV s^{-1}. Reproduced with permission from (2017) RSC [45].

surface charge separation at the electrode/electrolyte interface (*i.e.*, electrochemical double layered capacitive behavior) and surface Faradic redox reactions (*i.e.*, pseudocapacitive behavior). It is known that carbon/graphite materials have excellent electrochemical double-layered capacitive behavior, while transition metal oxides, conductive polymers, and carbon materials doped with hetero-atoms exhibit pseudocapacitive behavior [138–140]. Owing to the advantages of large internal surface area, small pore size, light weight, good electrical conductivity, high thermal/chemical stability, and outstanding mechanical properties, the carbon-containing 3D nanostructures including carbon nanofibers sponge [10], carbon nanotube networks [11], and graphene aerogels [35] have been considered as the most promising electrode materials for supercapacitors. The interconnected architecture not only shortens the transport distances for ions but also provides the continuous pathways (thus allowing for fast electron transport).

Lai *et al.* [45] developed an interesting type of carbon aerogel with unique cellular structure, consisting of 1D carbon nanofibers derived from oxidized PAN (o-PAN) and 2D carbon sheets originated from PI (Fig. 23A1). The o-PAN/PI (oPP) carbon aerogel with interconnected architecture demonstrated low density (Fig. 23A2) while improved mechanical strength (Fig. 23A3), and it could act as an ideal template for *in situ* growth of MnO_2 nanosheets to obtain oPP@MnO_2 hybrid carbon aerogel (Fig. 23B). The oPP-33.3@MnO_2-2h hybrid carbon aerogel showed the rectangular CV curve with the largest proportions (Fig. 23C1), indicating excellent rate stability. The oPP@MnO_2 aerogel possessed extraordinary electrochemical characteristics with maximum specific capacitance of 1066 F g^{-1}, which was close to the theoretical value of MnO_2 (1370 F g^{-1}). Additionally, the oPP-33.3@MnO_2-2h hybrid carbon aerogel had the high capacitance of 113.2 F g^{-1} at the scan rate of 200 mV s^{-1} (Fig. 23C2), and it also had the high retention of 92.4% after 5000 cycles (Fig. 23C3), indicating the outstanding long cycling stability. The successful fabrication of oPP carbon aerogels have broadened the scope of traditional electrospun membranes to 3D aerogels, providing a new strategy for the construction of nanofiber-based materials in energy storage application. In another study from the same group, Huang *et al.* [54] reported an efficient surface-induced co-assembly strategy to prepare graphene/carbon nanofiber (CNF) composite aerogels (GCA) with hierarchical structures by utilizing graphene flakes as cross-linkers. Owing to the largely increased surface area and charge-transfer efficiency derived from the firm interconnections among graphene flakes and CNFs, the prepared GCA demonstrated prominent capacitive performance as supercapacitor electrode.

To further improve the performance of electrospun 3D structures as supercapacitor electrode materials is to make suitable pores in the electrospun carbon nanofibers through chemical/physical activation. The activation process is able to result in the formation of nanopores and mesopores in nanofibers, which are desired for supercapacitor applications. In specific, nanopores would lead to high specific surface area thus benefit the large capacitance, while mesopores would provide enhanced electrolyte penetration for high power density [141]. Another approach is to develop electrospun 3D structures from transition metal oxide/sulfide nanofibers and conducting polymer nanofibers. Zhang *et al.* [142] developed 3D highly conductive and elastic electrospun PAN/PVP based CNFs

aerogel (PVP as a solder to weld adjacent nanofibers) by freeze drying, carbonization, and CO_2 activation for supercapacitor anode material. During the CO_2 activation at 900 °C, a fraction of carbon was burned off in the presence of CO_2 at the high temperature, resulting a high specific surface area of 437.2 $m^2\ g^{-1}$. The activated 3D anode material exhibited a high specific capacitance of 300 F g^{-1} at 0.3 A g^{-1}. Furthermore, the CNF surfaces were decorated by carbon nanotubes (CNTs) with the catalyst of metallic Co NPs, which were oxidized *in situ* to Co_3O_4 nanoparticles. The CNF-CNT-Co_3O_4 hybrid aerogel as a hierarchical cathode showed a high specific capacitance of 2376 F g^{-1} at 1 A g^{-1}. By assembling the activated CNF aerogel as anode and the hybrid aerogel as cathode, the asymmetric supercapacitor exhibited a considerably high energy density of 48.1 W h kg^{-1} at 780.2 W kg^{-1}.

4.2.2. Pressure sensor

Development of lightweight, flexible, and wearable sensors for biomedical applications (*e.g.*, electronic skins, real-time healthcare monitoring devices, prosthetics, and soft robotics) have attracted great interests [143-147]. Tactile pressure sensor, an essential sensory component for mapping of mechanical stimuli, measures the change of electric characteristics such as resistivity in response to mechanical force/deformation. 3D porous and conductive materials such as conductive aerogel/sponge of carbon nanotube [148,149] and graphene [150,151] have been recently studied as pressure sensors. However, these 3D materials typically possess either large (tens of micrometers) or small (several micrometers or smaller) pores but not both, whereas the hierarchical structures that process wide pore size distributions from small to large pores are desired for wide strain range strain/pressure sensors. Recently, Si *et al.* [52] developed super-elastic and pressure-sensitive carbonaceous nanofibrous aerogels with honeycomb-like structure through the combination of sustainable konjac glucomannan biomass and flexible SiO_2 nanofibers. The aerogels could sense dynamic pressure with a wide pressure range and high sensitivity, which enabled real pressure signals (*e.g.*, human blood pulses) to be monitored *in situ*. In another study, the polyimide-derived carbon nanofiber aerogels with high fatigue resistance and excellent flexibility were made by using the designed "fiber gluing" [152], and the resulting aerogels exhibited high performances as piezo-resistive stress sensors. Nevertheless, the conductivities of these aerogels were determined by carbonization process, and might not be precisely controlled/adjusted. In the case of compressive strain sensor, very high conductivity could lead to small change of conductivity thus low sensitivity during the sensing application.

We have reported a new method to prepare highly porous 3D sponges with tunable conductivity for making tactile pressure sensors [46]. The PAN and PI nanofibers provided mechanical resilience for the 3D conductive sponge, while the CNFs provided tunable electric conductivity. Upon varying the amounts of CNFs, the resistance of the 3D nanofibrous sponge could be readily tailored from ~260 kΩ to ~200 Ω. Under compressive strain, the resulting sensors based on these sponges had high sensitivity over a wide range of compressive strain (Fig. 24A1 & A2) as well as superior durability and stability (Fig. 24B). The tactile pressure sensor array (Fig. 24C1-C3) of electrospun 3D conductive sponge represented the state-of-art applications of these materials, indicating that these 3D conductive sponges might be promising materials in the design of highly sensitive tactile sensing devices. Furthermore, this method provides a new approach for the design of 3D porous materials with a variety of properties by incorporating functional

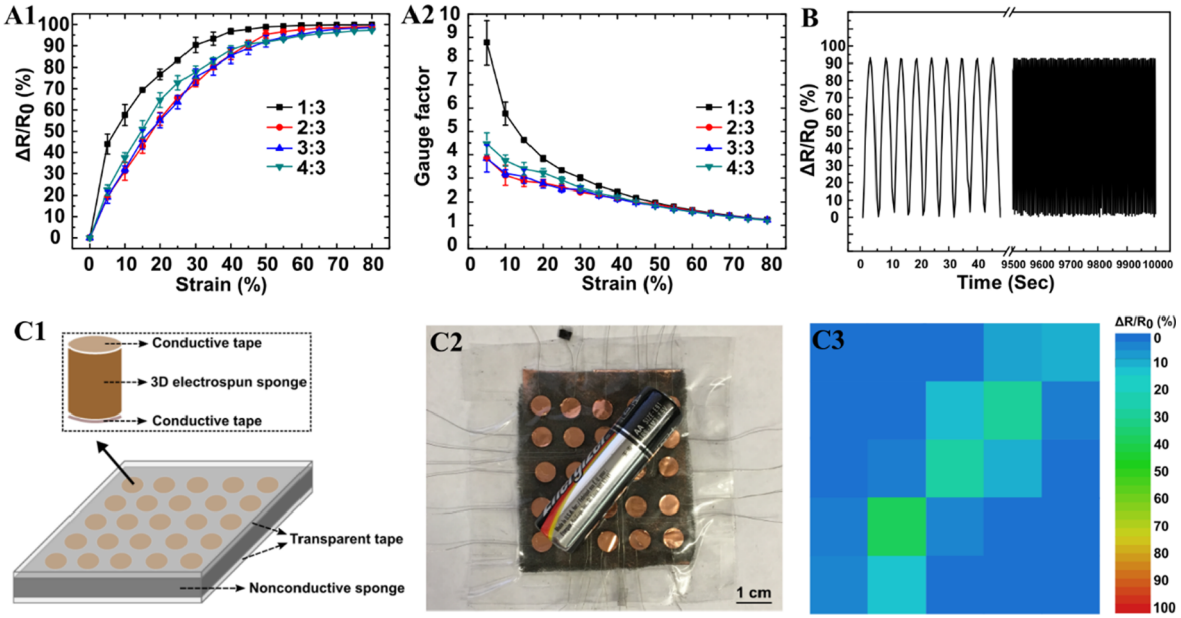

Fig. 24. (A1-A2) $\triangle R/R_0$ changes (A1) and gauge factor variations (A2) of 3D conductive sponges under different compressive strains. (B) The resistance change of the 3D conductive sponge (the sample with the CNFs-to-PAN/PI ratio of 1 to 3) under continuous compression and release between 50% and 0% strains for 10,000 s. (C1) Schematic of a proof-of-concept matrix of the sensor array, containing 5 pixel × 5 pixel pressure sensor units. (C2) Photograph of the sensor array with a battery placed on top. (C3) 2D mapping of the resistance changes corresponding to the pressure applied by the battery on the sensor array. Reproduced with permission from (2017) RSC [46].

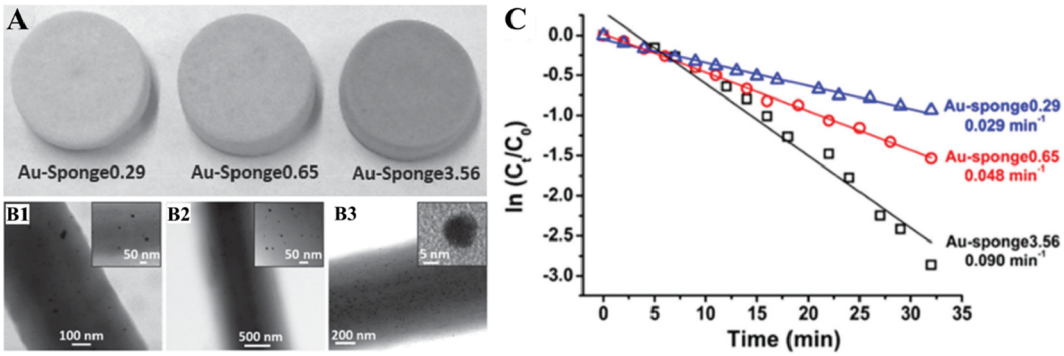

Fig. 25. (A) Photograph of the sponges with different amount of AuNPs; (B1-B3) TEM images of different amounts of AuNPs immobilized on nanofibers of the sponges (B1) 0.29 wt%, (B2) 0.65 wt%, and (B3) 3.56 wt%. (C) Pseudo-first-order plot of $\ln(C/C_0)$ versus time and the corresponding rate constant values for the reduction of 4-nitrophenol by Au-sponges. Reproduced with permission from (2016) Wiley [64].

materials and fragmented nanofibers as building blocks.

4.3. Chemical engineering

4.3.1. Catalyst carrier

The development of heterogeneous catalysts based on metal nanoparticles has attracted intensive attention, due to the increasing selectivity and catalytic activity by controlling pore size and particle characteristics [153]. Unfortunately, metal nanoparticles have a tendency to agglomerate, and further form large particles with low catalyst efficiency. To prevent/mitigate the aggregation and improve the catalysis efficiency, metal nanoparticles are usually dispersed and attached to robust supports with high specific surface areas. Duan *et al.* [64] immobilized gold nanoparticles (AuNPs) in a sponge made of short electrospun nanofibers (Fig. 25A), and the AuNPs were uniformly distributted and immobilized on the nanofiber surface (Fig. 25B). The resulting Au-sponge showed very low densities around 7 mg cm^{-3} (corresponding to the pore volume at about 150 mL g^{-1}), low surface area, and very low amount of AuNPs in the range of 0.29–3.56 wt%; and it had surprisingly high reaction rates at the extremely low gold amount (Fig. 25C), which was discerned as an extremely efficient catalyst (*i.e.*, even superior to other systems with dispersed AuNPs). The Au-sponge could also be reused up to five cycles for new reductions and thereby provided a sustainable catalyst design.

4.3.2. Thermal insulator and Joule heater

Thermally insulating sponges with tunable density, high thermal and mechanical stability, and desired elasticity are required for demanding applications. Jiang *et al.* [47] fabricated hierarchically structured sponges with bimodal interconnected pores, high porosity (> 99%), and tunable densities (between 7.6 and 10.1 mg cm^{-3}) by using PI as high temperature stable polymer and PAA as binder. To achieve high mechanical stability without sacrificing thermal properties, the "self-gluing" method was applied to bind the nanofibrous network skeleton of PI. The sponges with the density of 10.1 mg cm^{-3} showed low thermal conductivity of 0.026 W mK^{-1} and thermal diffusivity of 1.009 mm^2 s^{-1} (Fig. 26A). The sponges were compressible for at least 10,000 cycles and demonstrated good thermal insulation at high compressions. As shown in Fig. 26B, a hot iron plate (~376 °C) can be held on hand with the assistance of the PI sponge, and the gradient distribution of temperature from the plate to the sponge was observed when putting the PI sponge on the heating plate (~400 °C) (Fig. 26C & D). This superior thermal insulation made the PI sponges an ideal candidate for various high temperature applications (*e.g.*, firefighter protector, high-temperature filtration, sensors, and catalyst carrier for high-temperature reactions). In a follow-up study, Jiang *et al.* [119] developed the stress-responsive and electrically conductive nanocomposite sponges made of short electrospun PI nanofibers and Ag nanowires (AgNWs). The PI/Ag sponge possessed high electrical conductivity due to the excellent conductivity of AgNWs. The electrical conductivity of the sponge was increased upon compression, which was attributed to the percolation increase of AgNWs. Hence, the sponges could be applied directly as electrodes as well as very efficient Joule heaters. The heating and cooling rates were very fast, and that the maximum temperature reached by electric heating depended on the compressive strain. The PI/Ag sponge is expected to result in a new area for 3D sponge based conductive devices.

Ceramic sponges are ideal materials for thermal insulation, owing to their low thermal conductivity and good heat resistance performance. However, the development of flexible and super-elastic ceramic sponge is still a technological challenge, because the micro-architectural cellular structures made of traditional nanoceramics and nanoceramic composites are typically brittle [154]. To solve this problem, Si *et al.* [120] developed a scalable strategy to fabricate super-elastic ceramic nanofibrous aerogels (CNFAs) through combining SiO_2 nanofibers with aluminoborosilicate matrices. The resulting CNFAs had temperature-invariant super-elasticity, robust fire resistance, and thermal insulation performance. In a follow-up study, Dou *et al.* [155] developed a hierarchically structured silica nanofibrous aerogel by using electrospun SiO_2 nanofibers and SiO_2 nanoparticle aerogels as the building materials and SiO_2 sol as the high-temperature nanoglue. The acquired ceramic nanofibrous aerogel exhibited ultralow thermal conductivity (23.27 mW m^{-1} K^{-1}) and temperature-invariant super-elasticity from −196 to 1100 °C, making it ideal for thermal insulation applications.

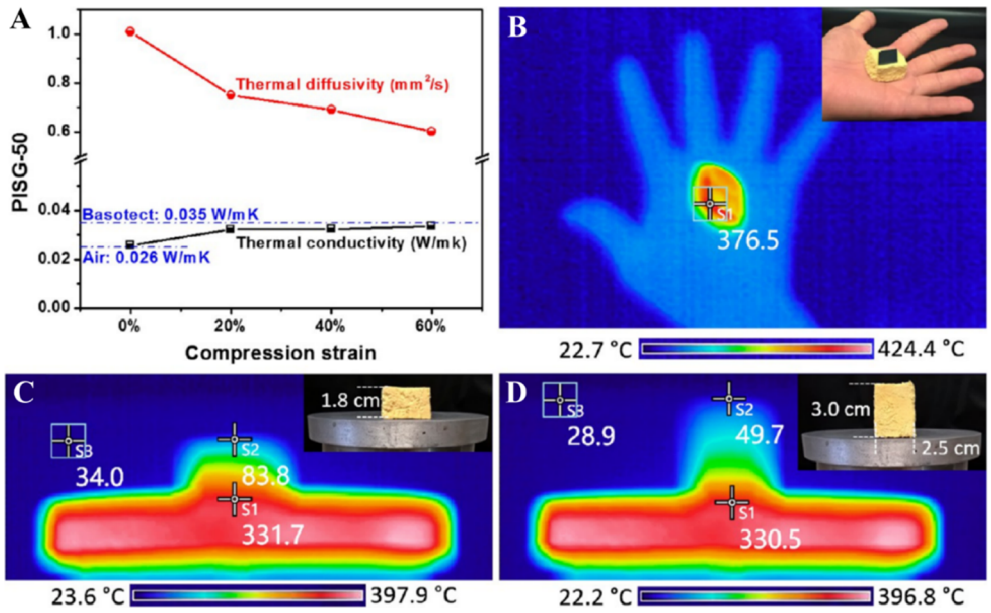

Fig. 26. (A) Thermal conductivity and thermal diffusivity of PISG-50 at different compression strain. Infrared (IR) camera images showing the thermal insulation of PI sponge: (B) A hot iron plate (~376 °C) was hold on hand with the assistance of the PI sponge, and the PI sponge with thickness of (C) 1.8 and (D) 3.0 cm on the heating plate (~400 °C). Insets showing the normal photos for the IR camera images. The sample size was 1.8 × 2.5 × 3.0 cm^3. Reproduced with permission from (2017) ACS [47].

4.4. Biomedical engineering

4.4.1. Tissue engineering scaffold

4.4.1.1. Bone tissue engineering scaffold. The worldwide incidence of bone disorders and conditions remains a significant clinical challenge. The engineered bone tissue has been considered as an alternative treatment strategy to replace autogenous and allogenous bone grafts [156,157]. In a natural bone tissue, the extracellular matrix (ECM) composed of organic collagen nanofibers and inorganic nano-hydroxyapatite provides structural support for cells and regulates a variety of cell functions, such as assembling cells, as well as regulating cell growth and cell-cell communication [158]. Therefore, the tissue engineering scaffolds have been extensively studied to mimic the critical features of natural ECMs, including chemical composition, structural organization, and mechanical properties [159,160]. However, the traditional electrospinning technique has the difficulty in directly producing clinically relevant 3D nanofibrous scaffolds with desired structural properties. To address this challenge, we have developed an innovative technique of thermally induced (nanofiber) self-agglomeration (TISA), a process by which as-electrospun PCL nanofiber membranes/mats can be converted into 3D electrospun PCL nanofibrous structures/scaffolds with interconnected macroporous structures [33]. Ensuing *in vitro* and *in vivo* data indicated that these novel scaffolds possess excellent capability to support BMP2-induced osteogenic differentiation and bone formation; however, only limited new bone was identified in the surrounding area of scaffolds. Consequently, our another work explored to improve the bioactivity of PCL scaffolds through introducing polylactic acid (PLA), the PCL/PLA-3D scaffolds demonstrated the substantially improved mechanical properties and bioactivity [50]. Although the PCL/PLA-3D scaffolds significantly promoted more osteogenic differentiation *in vitro* and new bone formation *in vivo* than PCL-3D scaffolds, the bone forming ability of the blend scaffolds are still limited and not able to completely heal the critical-sized bone defect even after the addition of rhBMP2. These results suggest that the biomimicking functionalizations/characteristics of these synthetic biopolymers (*i.e.,* PCL and PLA) have to be enhanced to create more bone-forming favorable microenvironment for improving the signaling activity of BMP2 and bone regeneration.

In our up-to-date work, we investigated the capabilities of 3D PCL nanofibrous scaffolds modified with mineral-mimicking hydroxyapatite (HA) in combination with BMP2 activator phenamil and their effects on osteogenesis *in vitro* and bone formation *in vivo* [96]. Bone-like HA is a commonly adopted and well tested modification for bone tissue engineering scaffolds, as it mimics the biphasic structure of natural bone [161], and has shown to positively impact BMP2 signaling *via* improved release kinetics and new bone formation in rats/mice [162,163]. Another strategy for improving BMP2 signaling is activating the endogenous BMP signaling pathway by using small molecules such as phenamil to act as the synergizing agent, which can reduce the required dosage thus be cost-effective [164–166]. We, therefore, hypothesized that functionalization of 3D PCL nanofibrous scaffolds with bone-like HA and BMP2 signaling activator phenamil will provide a favorable osteogenic niche for bone formation at low dose of BMP2. Compared to PCL-3D scaffolds, PCL/HA-3D scaffolds demonstrated synergistically enhanced osteogenic differentiation capabilities of C2C12 cells with phenamil. It is important to note that *in vivo* studies showed this synergism was able to generate significantly increased new bone in an ectopic mouse model (Fig. 27), suggesting that the PCL/HA-3D scaffold could act as a favorable synthetic extracellular

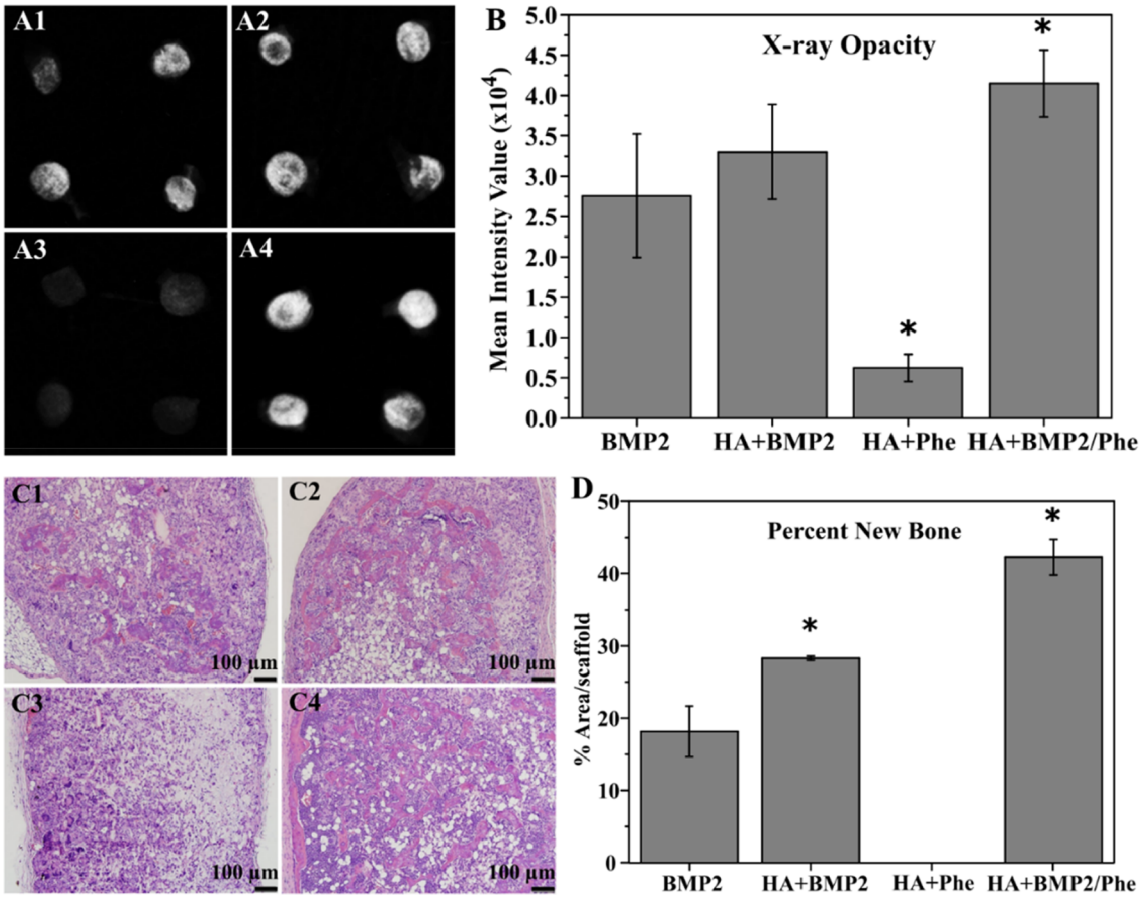

Fig. 27. (A1–A4) Radiographic examination of ossicles after harvesting from mice after 4 weeks. BMP2 only group (A1), BMP2 + HA group (A2), phenamil + HA group (A3), and BMP2/phenamil + HA group (A4) were all imaged, and mean intensity value of scaffolds was quantified (B). Data are expressed as mean ± SD (n = 4). (C1–C4) H&E staining of retrieved ossicles after 4 weeks implantation *in vivo*. BMP2 only group (C1), BMP2 + HA group (C2), phenamil + HA group (C3), and BMP2/phenamil + HA group (C4) area of new bone was measured by ImageJ software (D). Reproduced with permission from (2017) Elsevier [96].

matrix for bone regeneration.

Other groups also studied electrospun 3D scaffolds for bone tissue engineering. For example, Weng *et al.* [123] developed ultralight 3D hybrid nanofiber aerogels from shortened electrospun PLGA-collagen-gelatin nanofibers and electrospun bioactive glass nanofibers co-doped with Sr and Cu, followed by loading the resulting 3D aerogels with heptaglutamate E7 domain specifc BMP2. The nanofiber aerogels were surgically implanted into critical-sized defects created in rat calvariae. The hybrid aerogel exhibited sustained release of E7-BMP2 peptide from the degradable hybrid aerogels, which significantly improved bone healing and defect closure over 8 weeks in comparison to unfilled defects. Moreover, histopathology data revealed a near complete nanofiber aerogel degradation along with improved vascularization of the regenerated tissue. In another study, Wang *et al.* [167] developed a biomimetic 3D ceramic fibrous scaffold with self-ftting capability and tailorable gradation by assembly of intrinsically rigid and structurally flexible electrospun SiO_2 nanofibers with chitosan as bonding agent (SiO_2 NF-CS) *via* freezing drying. The super-elastic SiO_2 NF-CS scaffolds self-fitted to mandibular defects in rabbits, and promoted bone formation in rat calvarial defect. Furthermore, the SiO_2 NF-CS scaffolds with gradient in SiO_2 nanofbers had functional consequences, leading to a gradient in stiffness and hMSC differentiation into chondrocytes and osteoblasts spatially. The researchers from the same group [168] also developed flexibile bioactive glass (SiO_2–CaO) nanofibers and further assembled them into 3D fibrous scaffolds by using chitosan as linker. Upon implantation, the elastic fibrous scaffolds self-deployed and fitted into the irregularly shaped bone defects. Notably, the $85SiO_2$–15CaO/chitosan scaffolds demonstrated substantial promotion of bone regrowth and vascularization in the osteoporotic calvarial defect in a rat model.

4.4.1.2. Cartilage tissue engineering scaffold. Cartilage possesses low capacity for spontaneous healing and is extremely difficult to repair due to the avascular nature of the tissue. The treatment of cartilage injury, degeneration, and defects represent a critical clinical challenge, while none of currently available cartilage treatments can provide a satisfiable solution [169,170]. Recently, cartilage tissue engineering has been demonstrated to have tremendous clinical potential. Chen *et al.* [121] developed a porous 3D

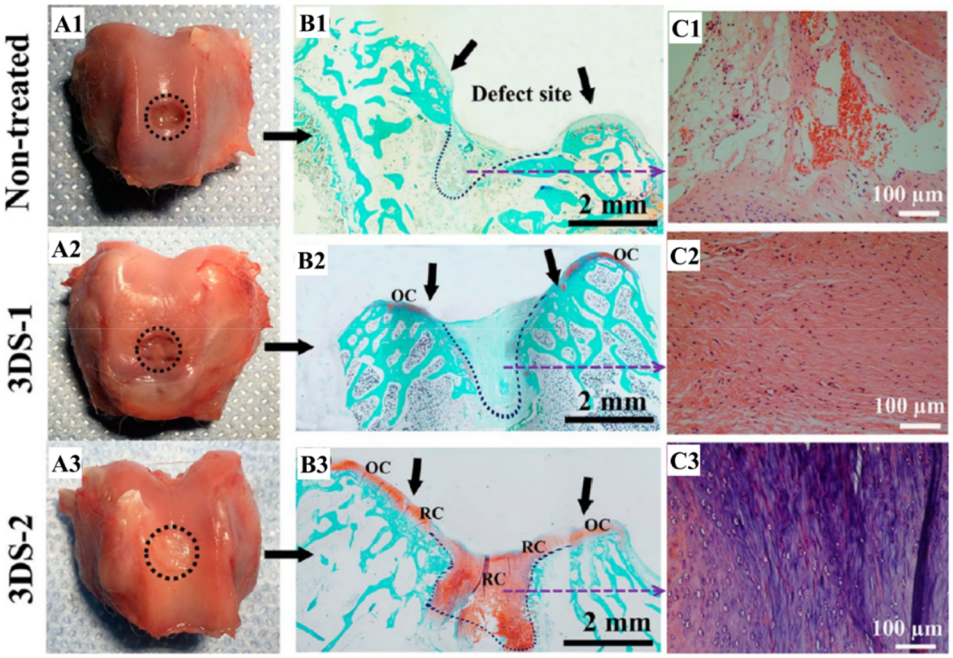

Fig. 28. Macroscopic images (A1, A2, and A3) of the cartilage joints from three groups at 12 weeks after surgery. Histological analysis of cartilage defect area from three groups at 12 weeks after surgery, stained with Safranin O-fast green (B1, B2, and B3) and H&E (C1, C2, and C3). Arrows and dotted lines indicating the defect sites. OC: original cartilage tissue. RC: repaired cartilage tissue. Reproduced with permission from (2017) ACS [121].

scaffold (3DS-1) assembled from shortened electrospun gelatin/PLA nanofibers for cartilage tissue regeneration. Additionally, the modified scaffold (3DS-2) crosslinked with hyaluronic acid (HA) was also fabricated to further enhance the repairing effect of cartilage. Both 3DS-1 and 3DS-2 scaffolds showed superabsorbent property and elastic property in the wet state. Chondrocytes were cultured on these 3D scaffolds, and both types of scaffolds demonstrated excellent cytocompatibility. Subsequently, the 3D scaffolds were applied to an *in vivo* cartilage regeneration study on rabbits by using an articular cartilage injury model. As shown in Fig. 28, the *in vivo* study revealed that the 3DS-2 scaffold could facilitate the repair of cartilage; hence, the developed 3D nanofibrous scaffold (3DS-2) would be promising for the cartilage tissue engineering application.

Structurally and functionally biomimetic tissue engineering scaffold is crucial to cartilage regeneration and cartilage defect repair. To improve the biological function of 3D electrospun scaffolds, Li *et al.* [171] developed the 3D composite biomimetic scaffolds by combining shortened electrospun gelatin-PCL nanofibers (NF) with decellularized cartilage extracellular matrix (DCECM). The nanofibers with the biomimetic microarchitecture of native cartilage served as skeleton and provided excellent mechanical properties, while the DCECM provided the biological micro-environment for the induction of cell response and promoted chondrocyte proliferation and early maturation of cartilages. *In vivo* results demonstarted that the composite nanofiber/DCECM scaffolds yielded better cartilage repair outcomes than those of the non-treated group and NF scaffolds group.

4.4.1.3. Nerve tissue engineering scaffold. Peripheral nerve injury is a common clinical problem. Nerve tissue engineering scaffold, also known as nerve guidance conduit with a cylindrical tube shape, represents a promising strategy to guide cells proliferation and facilitate axons extension of injured neural tissues in three dimensions, thus improving the functional recovery in peripheral nerve injury [172]. Artificial electrospun nanofiber nerve guides have attracted significant attention in bridging nerve gaps and associated peripheral nerve regeneration, owing to high surface area, flexibility, and porous structure [173]. Sun *et al.* [122] developed nanofiber sponges with abundant macropores, high porosity, and superior compressive strength by electrospinning and freeze-drying. Poly(L-lactic acid-co-ε-caprolactone)/silk fibroin (PLCL/SF) nanofiber sponges were used as filler to prepare 3D nanofiber sponge-containing (NS-containing) nerve guidance conduit (NGC). Compared to hollow NGC, the NS-containing NGC enhanced the proliferation of Schwann cells (SCs) due to the macroporous structure, and SCs infiltrated into the nanofiber sponges. Subsequently, the NS-containing NGC was implanted in a rat sciatic nerve defect model for evaluation *in vivo* (Fig. 29A). It was observed that the defect nerve was successfully bridged and regenerated upon implantation of the autologous nerve and NGCs for both 4 and 12 weeks (Fig. 29B). To prove the nerve function recovery of NGCs groups, the triceps surae muscles (TSM) of the defect nerve's target organ was sectioned for Masson staining. The images (Fig. 29C1) and quantitative analysis (Fig. 29C2) demonstrated that more collagen was deposited in hollow NGC group than NS-containing NGC, *i.e.*, the more serious loss of nerve function in hollow NGC which led to more severe myophagism and the greater amount of collagen enrichment, indicating the NS-containing NGC group performed better in nerve function recovery than the hollow NGC group. Moreover, the results of histological and morphological analyses, three indexes' immuno-histochemistry, and two indexes' immunofluorescence all indicated good nerve regeneration of NS-containing NGC

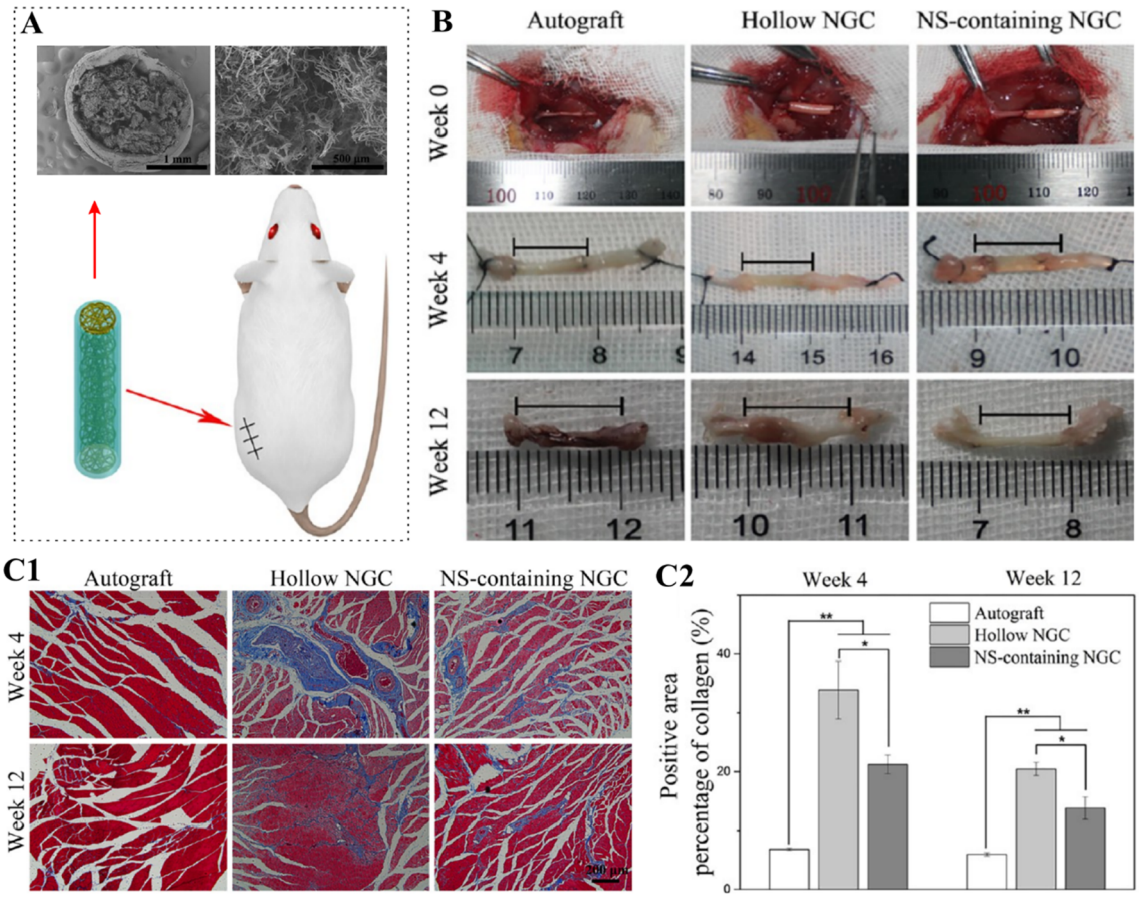

Fig. 29. (A) Schematic illustration of transplanting NS-containing NGC into SD rat sciatic nerve defect model. Insets: cross-section SEM images of NS-containing NGC in low (left) and high (right) resolution. (B) The gross observation of sciatic nerve after surgical procedures at week 0, and the regenerated sciatic nerve after implantation for 4 and 12 weeks (the scale bar = 10 mm, which marked the nerve defect site). (C1) Masson staining images of TSMs (experimental side) and (C2) statistical results of collagen positive area percentage after implantation for 4 and 12 weeks. Reproduced with permission from (2017) ACS [122].

as well, compared with hollow NGC. These results revealed that the NS-containing NGC had great potential in the application of peripheral nerve repair.

4.4.2. Hydrogel

Hydrogels are high water-containing hydrated networks with promising features including environmental friendliness, biocompatibility, anti-biofouling behavior, and responsiveness to external stimuli. Due to these distinguishing features, hydrogels have been widely applied as tissue engineering scaffolds and drug delivery vehicles [174–177]. However, in the ultrahigh-water-content region (above 97 wt%), the hydrogels usually become brittle and have small recoverable deformation due to high water contents and fragile networks in the fully swollen state. To address this issue, Si and co-workers [53] developed super-elastic, cellular-structured nanofibrous hydrogels (NFHs) by combining alginate and flexible SiO_2 nanofibers (Fig. 30A), in which naturally abundant and sustainable alginate was assembled into 3D elastic bulk NFHs. The resulting NFHs had ultrahigh water content (Fig. 30B), complete recovery from 80% strain, zero Poisson's ratio, shape memory behavior, injectability, and elastic-responsive conductivity. This study provided new insights for the design and development of multifunctional hydrogels. In another study, Jiang *et al.* [59] developed highly stable 3D PNIPAM sponges with temperature-dependent water uptake and release ability. These thermal responsive sponges can be used as smart water containers for the absorption and release of water upon changes in temperature. The sponges absorb high amounts of water (~7000%) at temperatures below the lower critical solution temperature (LCST) of PNIPAM and can release more than 80% of the absorbed water above the LCST in less than 2 min. Such spongy materials are very promising for water management, smart textiles, catalysis, and biomedical applications.

The innovative nanofiber-based hydrogels developed by the combination of traditional hydrogels and electrospun nanofibers have shown great potential in various research fields, because these hydrogels possess the superhydrophilicity, high water-holding capacity, good biocompatibility, enhanced mechanical strength, and excellent structural tunability. More information on nanofiber-based hydrogels has been provided in the recently published review paper from Ding's group [178].

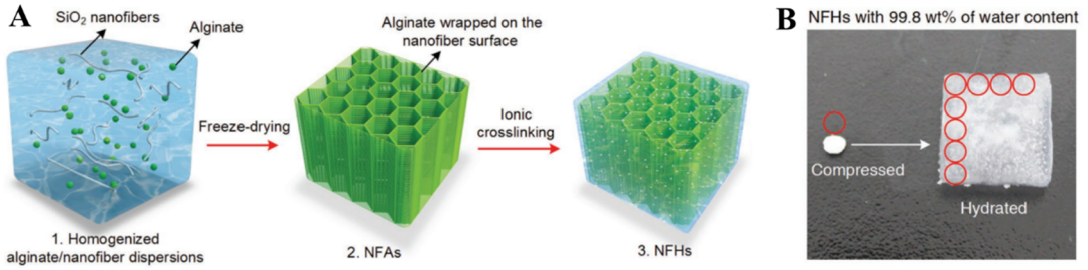

Fig. 30. (A) Schematic showing the synthetic steps. (1) Homogenized alginate/nanofiber dispersions were prepared through high-speed homogenization. (2) The dispersions were freeze-dried into alginate/nanofiber composite aerogels. (3) The resulting NFHs were fabricated by Al^{3+} crosslinking. (B) Photograph showing the water retention capacity of the NFHs. A sample of squashed and dried NFH of ~10 mg could hold ~5 g of water. Reproduced with permission from (2017) Wiley [53].

4.4.3. Drug delivery

In the field of drug delivery, achieving high drug loading capacity and controlling drug delivery are two main challenges. Duan *et al.* [179] developed polymeric macroporous sponges with very high pore volume and large porosity as a new type of drug carrier (Fig. 31A). Owing to the high pore volume (285 and 166 $cm^3\ g^{-1}$ for the sponges with densities being 3.5 and 6.0 mg cm^{-3}, respectively), the sponges had very high drug loading capacities with respective values of 1870 ± 114 and 2697 ± 73 mg g^{-1}, which are substantially higher than the meso and microporous drug carriers (< 1500 mg g^{-1}). To control the release profiles, an additional poly(p-xylylene) (PPX) coating was made by chemical vapor deposition on the drug-loaded sponge. Accordingly, artemisone (ART) release in the aqueous medium could be controlled by tailoring the density of the sponge and the thickness of the PPX coating (Fig. 31B). These 3D polymeric sponges would be highly beneficial as drug carriers for the programmed drug releasing to treat chronic diseases.

5. Concluding remarks and perspectives

In this review, we have systematically discussed the innovative strategies for the assembly of electrospun 3D nanofibrous structures/scaffolds/areogels, as well as their unique properties and various applications (summarized in Tables 1 & 2). Owing to the extremely high porosity, as well as the excellent structural flexibility and stability, these 3D nanofibrous structures have attracted significant interests for different applications, including environment (*e.g.*, organic compound removal, dye adsorption, and filtration and separation), energy (*e.g.*, supercapacitor), electronics (*e.g.*, pressure sensor), chemical engineering (*e.g.*, catalyst support, thermal insulator, and Joule heater), and biomedical engineering (*e.g.*, tissue engineering, hydrogel, and drug delivery). Nevertheless, this new topic area is still in the early stage; and further studies need to be carried out. In specific, future directions such as applying new materials, acquiring desired properties, and exploring high-value applications are suggested, as summarized below.

Thus far, numerous materials can be electrospun into nanofibers, while only a few have been assembled into 3D structures. Therefore, the primary future direction is to apply new materials into the 3D structures. For example, biologically derived polymers or synthetic polymers are feasible to be fabricated into the 3D tissue engineering scaffolds, while the biomass (*e.g.*, lignin) based 3D carbon nanofibrous structures are expected to be applied in environment and energy-related applications.

Another future direction is the development of new properties in 3D structures. For example, some innovative properties can be acquired through various modification and functionalization methods such as surface grafting (*e.g.*, surface-initiated controlled

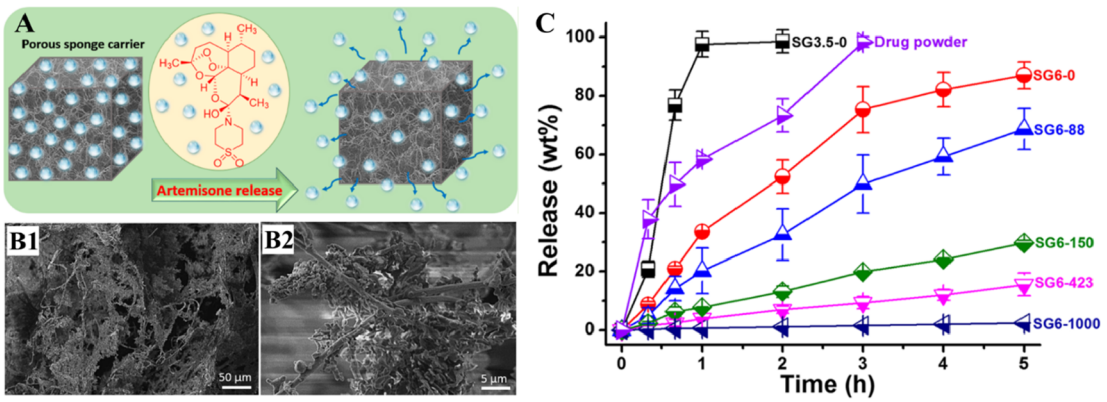

Fig. 31. (A) Schematic drawing for the ART release from porous sponge carrier. (B1 and B2) Cross-sectional SEM images of as-prepared sponge SG6 after loading with ART. (C) *In vitro* ART release from the ART powder and from sponges with different densities (3.5 and 6 mg cm^{-3}) and PPX coating thickness (0, 88, 150, 423, and 1000 nm). Reproduced with permission from (2017) ACS [179].

Table 1
Fabrication parameters and applications of 3D structures assembled from fragmented electrospun nanofiber mats/membranes.

Method	Nanofiber material	Binding agent	Dispersing liquid	Processing temperature	Post processing	Application	Ref.
Freeze drying-Ding's group	PAN & SiO_2	BAF-a	Water/*tert*-butanol	Liquid nitrogen (−196 °C)	Crosslinking at 240 °C, and calcination at 850 °C	Thermal insulation, sound absorption, oil-water separation	[31]
	PAN, SiO_2, & SiO_2 NPs	BAF-a	Camphene	Liquid nitrogen (−196 °C)	None	Oil/water emulsions separation	[62]
	SiO_2	KGM	Water	Liquid nitrogen (−196 °C)	Deacetylation of KGM at 90 °C, and calcination at 850 °C	Pressure sensor	[52]
	SiO_2	Alginate/Al^{3+}	Water	Dry ice/acetone (−77 °C)	Ionic crosslinking in metallic cations solution	Pressure sensor	[53]
	SiO_2	Aluminoborosilicate	Water with polyacrylamide	Dry ice/acetone (−77 °C)	Calcination at 900 °C	Thermal insulation	[120]
	SiO_2	PVA/Citric acid	Water	Liquid nitrogen (−196 °C)	Crosslinking at 120 °C	Protein separation	[136]
	SiO_2 nanofibers & NPs	SiO_2 sol	Water (PEO)	Liquid nitrogen (−196 °C)	Calcined at 700 °C	Thermal insulation	[155]
	SiO_2	Chitosan and glutaraldehyde	Water	−80 °C	Glutaraldehyde crosslinking	Bone tissue engineering	[167]
	SiO_2/Polyphosphoric acid (PPA)	Ethylene-vinyl alcohol copolymers (EVOH)	*tert*-Butanol/water	Not reported	Thermal crosslinking /phosphorylation	Protein separation	[137]
	SiO_2-CaO	Chitosan and glutaraldehyde	Water	−80 °C	Glutaraldehyde crosslinking	Osteoporotic bone regeneration	[168]
Greiner's group	PMMM/PAN	UV cross-linking	Dioxane	Not reported	None	Oil absorption, cell culture	[32]
	PMMM/PAN	UV cross-linking	Dioxane	Not reported	PPX CVD coating	Separation, heat insulation	[67]
	Poly(2VP-co-MABP)/PMMM/PAN	UV cross-linking	Dioxane	−20 °C	Au immobilization	Catalyst carrier	[64]
	PMMM/PAN	UV cross-linking	Dioxane	Not reported	PPX CVD coating	Spongy gel	[129]
	PMMM/PAN	UV cross-linking	Dioxane	Not reported	Drug loading and PPX coating	Drug carriers	[179]
	PI	PAA	Dioxane/DMSO	−20 °C	Thermal imidization	Thermal insulator	[47]
	PI & Ag nanowires	PAA	Dioxane/DMSO	−20 °C	Incorporation of Ag nanowires	Joule heaters	[63]
	PNIPAM	PNIPAM	Dioxane	−20 °C	UV cross-linking	Water absorption	[59]
	BBB	PVA	Dioxane	Not reported	Heat treatment at 500 °C	Flame retardant	[48]
	PI & Ketjen carbon black nanoparticles	PAA	Dioxane	Not reported	Thermal imidization	Thermal insulator	[66]
Liu's group	PAN	GO	Water	Liquid nitrogen (−196 °C)	Carbonization at 850 °C, $MoSe_2$	Energy storage/conversion	[54]
	PAN	PAA	Water	Liquid nitrogen (−196 °C)	Carbonization at 850 °C, MnO_2	Supercapacitor	[45]
	PI	PAA	Water	Liquid nitrogen (−196 °C)	Thermal imidization	Thermal insulator	[118]

(*continued on next page*)

Table 1 (*continued*)

Method	Nanofiber material	Binding agent	Dispersing liquid	Processing temperature	Post processing	Application	Ref.
Mo's group	Gelatin/PLA	Glutaraldehyde	*tert*-Butanol	−80 °C	None	Tissue engineering	[51]
	Gelatin/PLA	Gelatin/PLA blend	*tert*-Butanol	−20 °C	Thermal crosslinking at 190 °C	Cartilage tissue engineering	[121]
	PLCL/Silk fibroin	Glutaraldehyde	*tert*-Butanol	Not reported	None	Nerve tissue engineering	[122]
Adlhart's group	Pullulan/PVA	PVA	Dioxane	−80 °C	Thermal crosslinking, CVD coating	Liquid absorption	[113]
	Pullulan/PVA	PVA	Dioxane	−80 °C	Thermal crosslinking	Particle filters	[135]
	Pullulan/PVA/PAA	PVA/PAA	Dioxane	Not reported	Thermal crosslinking	Dye adsorption	[131]
Chang's group	PVASi	TEDB-NH_2	Toluene/DIPEA	Polymerization at 80 °C for 24 h	Soxhlet extraction and vacuum dry	Dye adsorption	[114]
Xu's group	PI	None	Dioxane	−4 °C	Thermal cross-linking	Particulate air filters	[60]
Xie's group	PLGA-Collagen-gelatin	PLGA	Water	−80 °C	Thermal treatment	Bone tissue engineering	[123]
Wang's group	SA/PAM	PMDA	Acetic acid	−20 °C	Chemical crosslinking	Ion adsorption	[134]
	PLA/regenerated cellulose (RC)	Citric acid	*tert*-Butanol/water	−20 °C	Thermal treatment	Biomineralization	[55]
Deng's group	PI	None	Water/*tert*-butanol	−20 °C, −80 °C and −196 °C	Solvent-vapour	Particle or aerosol filtration	[61]
Zhang's group	PI	PAA nanoparticles	*tert*-Butanol/water	−10 °C	Thermal imidization and carbonization	Piezoresistive stress sensors	[152]
Gu' group	Gelatin/PCL	decellularized cartilage ECM	*tert*-Butanol (1.5% w/v)	−20 °C	Cross-linking in an ethanol solution	Cartilage tissue engineering	[171]
Yu	PAN/polyvinylpyrrolidone (PVP)	PVP	*tert*-Butanol/water	−80 °C	Pre-oxidation, carbonization and CO_2 activation	Supercapacitor	[141]
Fong's group	PAN, PI, & CNFs	PVA	Water/ethanol	Liquid nitrogen (−196 °C)	Thermal stabilization at 230 °C	Pressure sensor	[46]
	RC	PVA	Water/ethanol	Liquid nitrogen (−196 °C)	Thermal stabilization at 230 °C	Organic compounds absorption	[49]
	PAN, PI, & HNTs	PVA	Water/ethanol	Liquid nitrogen (−196 °C)	Thermal stabilization at 230 °C	Dye adsorbent and catalyst support	[65]
TISA- Fong's group	PCL	PCL	Water/ethanol/gelatin	55 °C	N/A	Bone tissue engineering	[33]
	PCL/PLA (80/20, wt./wt.)	PCL	Water/ethanol/gelatin	54 °C	N/A	Bone tissue engineering	[50]
	PCL/PLA (different wt. ratios)	PCL	Water/ethanol/gelatin	52–65 °C	Thermal stabilization	Bone tissue engineering	[69]
	PCL & HA	PCL	Water/ethanol/gelatin	55 °C	Functionalization with HA and phenamil	Bone tissue engineering	[96]
	CA/PCL	PCL	Water/ethanol	75 °C	Thermal stabilization	Drug delivery and tissue engineering	[68]

Table 2
Properties of 3D structures assembled from fragmented electrospun nanofiber mats/membranes.

Method	Nanofiber material	Density (mg cm^{-3})	Porosity (%)	Pore size (μm)	BET (m^2 g^{-1})	Stress @ 50% (kPa) & cycles	Thermal conductivity (W mK^{-1})	Electrical conductivity (S cm^{-1})	Water contact angle (°)	Ref.
Freeze drying-Ding's group	PAN and SiO_2	0.12–9.6	99.992–99.36	~20 & ~1	N/A	~7.5 & 1000	0.026	0.25	145	[31]
	PAN, SiO_2, and SiO_2 NPs	13.76–29.94	98.94–97.69	18.94–4.16	2.66–76.54	~15 & 1000	N/A	N/A	138–162	[62]
	SiO_2 and KGM	5.2	99.9	~20 & ~1	N/A	~4 & 1000	N/A	0.21	N/A	[52]
	SiO_2 and Alginate	N/A	99	~20 & ~1	N/A	~6 & 1000	N/A	1.85	Hydrophilic	[53]
	SiO_2	0.15	99.993	10–30 & 0.1–1	N/A	~4 & 500	0.032–0.025	N/A	N/A	[120]
	SiO_2 and PVA	1.8	98.4–99.5	50–200 & 1–2	N/A	~5 & 1000	N/A	N/A	Hydrophilic	[136]
	SiO_2 nanofibers & NPs	0.2	> 99.9	50	N/A	~3 & 1000	0.023	N/A	N/A	[155]
	SiO_2 and Chitosan	N/A	N/A	30–140	N/A	~6 & 10,000	N/A	N/A	Hydrophilic	[167]
	SiO_2/PPA	17.5–21.2	98.75–98.85	2–26	N/A	~6 & 1000	N/A	N/A	Hydrophilic	[137]
	SiO_2-CaO/chitosan	25	N/A	70–220 & 1–2	N/A	~15 & 1000	N/A	N/A	Hydrophilic	[168]
Greiner's group	PMMM/PAN	2.72–9.12	99.6	300–430 & 10–30	2.66	~0.3–0.9 & N/A	N/A	N/A	Hydrophobic	[32]
	PolyMMMM/PAN & PPX	4.83–22.59	N/A	N/A	N/A	0.81–12.13 & 1000	0.05	N/A	119–156	[67]
	Poly(2VP-co-MABP)/PMMM/PAN & PPX-Au	7	> 99	50–400 & ~10	N/A	N/A	N/A	N/A	N/A	[64]
	PMMM/PAN & PPX	16.2 & 30.6	98.3 & 97.9	N/A	N/A	N/A	N/A	N/A	148 & 142	[129]
	PMMMM/PAN & PPX-Artemisone	3.5 & 6.0	99.7 & 99.5	~100 & < 10	1	N/A	N/A	N/A	Hydrophobic	[179]
	PI	7.6–10.1	99.46–99.28	73–121 & < 10	N/A	1.15–2.20 & 10,000	0.026–0.033	N/A	N/A	[47]
	PI &Ag nanowires	40.6	98	121 & < 10	N/A	3.6 & 10,000	0.07–0.1036	1.70	N/A	[63]
	PNIPAM	4.10–21.04	> 98	~10–100	N/A	1.2×10^{-3}	N/A	N/A	Hydrophilic	[59]
	BBB & PVA	2.9–13.9	> 99	100 & 5–10	N/A	0.5 & 6	0.028–0.038	N/A	149.8	[48]
	PI & Ketjen carbon black nanoparticles	12–22	98–99	100 & < 10	N/A	5.5 & 5000	0.028–0.032	N/A	Hydrophobic	[66]
Liu's group	PAN/GO	4.8	N/A	< 10	N/A	5 & 30	N/A	0.0926	N/A	[54]
	PAN/PAA	N/A	N/A	< 10	N/A	N/A	N/A	N/A	Hydrophobic	[45]
	PI/PAA	54.4	96.1	50	N/A	170	0.039	N/A	N/A	[118]
Mo's group	Gelatin/PLA	76.6–138.8	N/A	100–500 & 20	N/A	0.03 & 100	N/A	N/A	Hydrophilic	[51]
	Gelatin/PLA	94.8 & 103	N/A	200 & 20	N/A	400	N/A	N/A	Hydrophilic	[121]
	PLCL/Silk fibroin	N/A	88.81	1–100	N/A	10 & 100	N/A	N/A	Hydrophilic	[122]

(*continued on next page*)

Table 2 (*continued*)

Method	Nanofiber material	Density (mg cm^{-3})	Porosity (%)	Pore size (μm)	BET (m^2 g^{-1})	Stress @ 50% (kPa) & cycles	Thermal conductivity (W mK^{-1})	Electrical conductivity (S cm^{-1})	Water contact angle (°)	Ref.
Adlhart's group	Pullulan & PVA	12.64–92.27	99.13–93.65	50–100 & 2–5	N/A	4.5 & 50	N/A	N/A	136	[113]
	Pullulan & PVA	23.2–88.5	98.40–93.91	50–100 & 2–5	N/A	N/A	N/A	N/A	N/A	[135]
	Pullulan/PVA/PAA	24.5	98.2	20–40 & 2–5	N/A	N/A	N/A	N/A	Hydrophilic	[131]
Chang's group	PVASi-NH_2	30.4	N/A	< 10	447	30 & 10	N/A	N/A	Hydrophobic	[114]
Xu's group	PI	4.6–13.1	99.0–99.6	50–100 & < 1	12.4	~1 & 1000	0.0297–0.0318	N/A	N/A	[60]
Xie's group	PCG & BG	N/A	N/A	30	N/A	N/A	N/A	N/A	Hydrophilic	[123]
Wang's group	SA/PAM	50.6	N/A	10–50 & 1–5	N/A	12 & 100	N/A	N/A	0	[134]
	PLA/RC	32.5–33.8	95.9–96.1	50–150 & < 20	N/A	13 & 100	N/A	N/A	84.7°	[55]
Deng's group	PI	4.81	99.66	~100 & < 10	N/A	~2 & 100	N/A	N/A	N/A	[61]
Zhang's group	PI	6.6	> 99	1–3	N/A	8.9 & 1000	0.0266–0.0304	N/A	N/A	[152]
Gu' group	Gelatin/PCL & decellularized cartilage ECM	N/A	N/A	200–300 & > 10	N/A	~10	N/A	N/A	Hydrophilic	[171]
Yu	PAN/PVP	14.8	N/A	~5	437.2	80 & 100	N/A	3.25	N/A	[141]
Fong's group	PAN, PI, & CNFs	6.84–12.41	99.44–99.12	~100 & ~1	N/A	~2–6 & 2000	N/A	Tunable conductivity	N/A	[46]
	RC	6.45	99.57	~20 & 2	N/A	~2	N/A	N/A	141.2	[49]
	PAN, PI, & HNTs	33.2–88.4	97.9–95.3	~20 & 2	14.5–27.8	N/A	N/A	N/A	Hydrophilic	[65]
TISA-Fong's group	PCL	41	96.4	300 & 2	N/A	N/A	N/A	N/A	Hydrophilic	[33]
	PCL/PLA (80/20, wt./wt.)	48	95.8	300 & 2	N/A	N/A	N/A	N/A	Hydrophilic	[50]
	PCL/PLA (different wt. ratios)	47.1–12.6	95.9–99	300 & 2	N/A	N/A	N/A	N/A	Hydrophilic	[69]
	PCL & HA	N/A	N/A	300 & 2	N/A	N/A	N/A	N/A	Hydrophilic	[96]
	CA/PCL	66	95	100 & 2	N/A	N/A	N/A	N/A	136.5	[68]

radical polymerization), surface coating (*e.g.,* hydrothermal reaction, layer-by-layer self-assembly), incorporating nanofillers (*e.g.*, 0D, 1D, and 2D nanomaterials) into nanofibers, and attaching nanomaterials on the nanofiber surfaces. Furthermore, developing specially structured nanofibers such as nanoporous nanofibers, hollow nanofibers, and 3D aligned nanofibers is another effective approach to provide the 3D structures with innovative properties.

The new applications of electrospun 3D structures need to be explored. For environment application, electrospun 3D structures are promising candidates for water purification (micro-, ultra-, and nano-filtration) and desalination (*e.g.*, direct solar desalination [180]). For energy application, the development of electrospun 3D conductive structures as novel electrodes for advanced energy conversion devices (*e.g.*, batteries, dye-sensitized solar cells, and microbial fuel cells) is promising. For electronics application, such 3D structures might be useful to develop sensors (*e.g.*, biosensor, gas sensor, and optical sensor) and detectors (*e.g.*, SERS detector). For chemical engineering application, one of the new applications is to use the 3D structures as adsorbents, which could be adopted for immobilization/adsorption of proteins (*e.g.*, enzyme). Furthermore, the 3D structures might also be applied as sound absorption materials. For biomedical engineering application, the 3D scaffolds have now been investigated/used in bone, cartilage, and nerve tissue engineering, and need to be further explored in various other tissue engineering areas, including but not limited to muscle, skin, myocardium, tendon, ligament, vascular, and dental. It is necessary to note that, although the 3D scaffolds assembled from electrospun short nanofibers are promising, they may not be suitable for every tissue engineering applications (*e.g.*, wound dressing). Since the 3D scaffolds consist of short nanofibers that tend to form debris under external pressure, the debris may remain in the wound, causing inflammation and increasing the risk of infection [24]. Therefore, more studies are needed to explore the potential application of 3D scaffolds in different tissue engineering areas.

Although electrospun 3D nanofibrous structures with unique properties may lead to exciting opportunities for many innovative applications, it appears that, how to scale up the productivity to fulfill commercialization requirements might be a challenge. This is because the difficulties on the electrospinning technology (*e.g.*, large-scale production, precise control of morphological/structural properties, and environmental/safety concerns) [181] remain as major restrictions; additionally, there are other technological challenges hindering the industry-scale production of 3D nanofibrous structures. These challenges include (1) the large-scale fabrication of morphologically uniform electrospun shortened/fragmented nanofibers and (2) the transfer of freeze drying or TISA processing methods from laboratory to industrial scale. Additionally, precisely controlling the lengths/sizes of shortened/fragmented nanofibers is also difficult. Researchers have encountered difficulties in the preparation of uniform nanofibers with diameters below 50 nm, and the fragmentation of electrospun nanofiber mats/membranes into uniform short nanofibers and/or tiny pieces in large scale is also challenging. Finally, the complexity of post-treatment and/or surface modification/functionalization for electrospun 3D nanofibrous structures might hinder the productivity as well.

Despite the above difficulties and challenges, researchers and entrepreneurs have been actively seeking to take electrospun nanofibrous materials from academic research to real-world applications. Thus far, there are at least 20 companies in the world that manufacture over 50 different types of electrospun nanofiber based products [181]. Owing to superior properties and wide applications of electrospun 3D nanofibrous structures, it is reasonable to expect that commercial products will become available in the future.

Declaration of Competing Interest

The authors declare that they have no known competing financial interests or personal relationships that could have appeared to influence the work reported in this paper.

Acknowledgements

This work was supported by the National Aeronautics and Space Administration (NASA Cooperative Agreement Number: 80NSSC18M0022), the EPSCoR program of U.S. National Science Foundation (Award Number: IIA-1335423), the Competitive Research Grant Program of South Dakota Board of Regents (Award Numbers: UP1500172 and UP1600205), and State of South Dakota. The authors would also like to acknowledge the Biomedical Engineering Program at the South Dakota School of Mines and Technology.

References

[1] Reneker DH, Yarin AL. Electrospinning jets and polymer nanofibers. Polymer 2008;49:2387–425.
[2] Agarwal S, Greiner A, Wendorff JH. Functional materials by electrospinning of polymers. Prog Polym Sci 2013;38:963–91.
[3] Peng S, Jin G, Li L, Li K, Srinivasan M, Ramakrishna S, et al. Multi-functional electrospun nanofibres for advances in tissue regeneration, energy conversion & storage, and water treatment. Chem Soc Rev 2016;45:1225–41.
[4] Li D, Xia Y. Electrospinning of nanofibers: reinventing the wheel? Adv Mater 2004;16:1151–70.
[5] Greiner A, Wendorff JH. Electrospinning: a fascinating method for the preparation of ultrathin fibers. Angew Chem Int Ed 2007;46:5670–703.
[6] Agarwal S, Wendorff JH, Greiner A. Progress in the field of electrospinning for tissue engineering applications. Adv Mater 2009;21:3343–51.
[7] Liu W, Thomopoulos S, Xia Y. Electrospun nanofibers for regenerative medicine. Adv Healthc Mater 2012;1:10–25.
[8] Xue J, Xie J, Liu W, Xia Y. Electrospun nanofibers: new concepts, materials, and applications. Acc Chem Res 2017;50:1976–87.
[9] Zhang L, Aboagye A, Kelkar A, Lai C, Fong H. A review: carbon nanofibers from electrospun polyacrylonitrile and their applications. J Mater Sci 2014;49:463–80.
[10] Chen L-F, Feng Y, Liang H-W, Wu Z-Y, Yu S-H. Macroscopic-scale three-dimensional carbon nanofiber architectures for electrochemical energy storage devices. Adv Energy Mater 2017;7:1700826.
[11] Nardecchia S, Carriazo D, Ferrer ML, Gutierrez MC, del Monte F. Three dimensional macroporous architectures and aerogels built of carbon nanotubes and/or

graphene: synthesis and applications. Chem Soc Rev 2013;42:794–830.
[12] Lavoine N, Bergström L. Nanocellulose-based foams and aerogels: processing, properties, and applications. J Mater Chem A 2017;5:16105–17.
[13] Jiang L, Fan Z. Design of advanced porous graphene materials: from graphene nanomesh to 3D architectures. Nanoscale 2014;6:1922–45.
[14] Li S, Cheng C, Thomas A. Carbon-based microbial-fuel-cell electrodes: from conductive supports to active catalysts. Adv Mater 2017;29:1602547.
[15] Jiang S, Agarwal S, Greiner A. Low-density open cellular sponges as functional materials. Angew Chem Int Ed 2017;56:15520–38.
[16] Sun B, Long YZ, Zhang HD, Li MM, Duvail JL, Jiang XY, et al. Advances in three-dimensional nanofibrous macrostructures via electrospinning. Prog Polym Sci 2014;39:862–90.
[17] Sun B, Jiang X-J, Zhang S, Zhang J-C, Li Y-F, You Q-Z, et al. Electrospun anisotropic architectures and porous structures for tissue engineering. J Mater Chem B 2015;3:5389–410.
[18] Taskin MB, Xu RD, Gregersen H, Nygaard JV, Besenbacher F, Chen ML. Three-dimensional polydopamine functionalized coiled microfibrous scaffolds enhance human mesenchymal stem cells colonization and mild myofibroblastic differentiation. ACS Appl Mater Interfaces 2016;8:15864–73.
[19] Li D, Wu T, He N, Wang J, Chen W, He L, et al. Three-dimensional polycaprolactone scaffold via needleless electrospinning promotes cell proliferation and infiltration. Colloids Surf B Biointerfaces 2014;121:432–43.
[20] Chang G, Zhu X, Li A, Kan W, Warren R, Zhao R, et al. Formation and self-assembly of 3D nanofibrous networks based on oppositely charged jets. Mater Des 2016;97:126–30.
[21] Tokarev A, Asheghali D, Griffiths IM, Trotsenko O, Gruzd A, Lin X, et al. Touch- and brush-spinning of nanofibers. Adv Mater 2015;27:6526–32.
[22] Vaquette C, Cooper-White J. A simple method for fabricating 3-D multilayered composite scaffolds. Acta Biomater 2013;9:4599–608.
[23] Jiang J, Li Z, Wang H, Wang Y, Carlson MA, Teusink MJ, et al. Expanded 3D nanofiber scaffolds: cell penetration, neovascularization, and host response. Adv Healthc Mater 2016;5:2993–3003.
[24] Zhang K, Bai X, Yuan Z, Cao X, Jiao X, Li Y, et al. Layered nanofiber sponge with an improved capacity for promoting blood coagulation and wound healing. Biomaterials 2019;204:70–9.
[25] Zhang D, Chang J. Electrospinning of three-dimensional nanofibrous tubes with controllable architectures. Nano Lett 2008;8:3283–7.
[26] Yeo M, Kim G. Cell-printed hierarchical scaffolds consisting of micro-sized polycaprolactone (PCL) and electrospun PCL nanofibers/cell-laden alginate struts for tissue regeneration. J Mater Chem B 2014;2:314–24.
[27] Kim MS, Son J, Lee H, Hwang H, Choi CH, Kim G. Highly porous 3D nanofibrous scaffolds processed with an electrospinning/laser process. Curr Appl Phys 2014;14:1–7.
[28] Lee J, Lee SY, Jang J, Jeong YH, Cho D-W. Fabrication of patterned nanofibrous mats using direct-write electrospinning. Langmuir 2012;28:7267–75.
[29] Cai Y-Z, Zhang G-R, Wang L-L, Jiang Y-Z, Ouyang H-W, Zou X-H. Novel biodegradable three-dimensional macroporous scaffold using aligned electrospun nanofibrous yarns for bone tissue engineering. J Biomed Mater Res A 2012;100A:1187–94.
[30] Ahirwal D, Hebraud A, Kadar R, Wilhelm M, Schlatter G. From self-assembly of electrospun nanofibers to 3D cm thick hierarchical foams. Soft Matter 2013;9:3164–72.
[31] Si Y, Yu J, Tang X, Ge J, Ding B. Ultralight nanofibre-assembled cellular aerogels with superelasticity and multifunctionality. Nat Commun 2014;5:5802.
[32] Duan G, Jiang S, Jérôme V, Wendorff JH, Fathi A, Uhm J, et al. Ultralight, soft polymer sponges by self-assembly of short electrospun fibers in colloidal dispersions. Adv Funct Mater 2015;25:2850–6.
[33] Xu T, Miszuk JM, Zhao Y, Sun H, Fong H. Electrospun polycaprolactone 3D nanofibrous scaffold with interconnected and hierarchically structured pores for bone tissue engineering. Adv Healthc Mater 2015;4:2238–46.
[34] Deville S, Saiz E, Nalla RK, Tomsia AP. Freezing as a path to build complex composites. Science 2006;311:515–8.
[35] Chabot V, Higgins D, Yu A, Xiao X, Chen Z, Zhang J. A review of graphene and graphene oxide sponge: material synthesis and applications to energy and the environment. Energy Environ Sci 2014;7:1564–96.
[36] Cheng C, Li S, Thomas A, Kotov NA, Haag R. Functional graphene nanomaterials based architectures: biointeractions, fabrications, and emerging biological applications. Chem Rev 2017;117:1826–914.
[37] Wu Z-Y, Liang H-W, Chen L-F, Hu B-C, Yu S-H. Bacterial Cellulose: A robust platform for design of three dimensional carbon-based functional nanomaterials. Acc Chem Res 2016;49:96–105.
[38] Han J, Zhou C, Wu Y, Liu F, Wu Q. Self-assembling behavior of cellulose nanoparticles during freeze-drying: effect of suspension concentration, particle size, crystal structure, and surface charge. Biomacromolecules 2013;14:1529–40.
[39] Deville S. Freeze-casting of porous ceramics: a review of current achievements and issues. Adv Eng Mater 2008;10:155–69.
[40] Deville S, Saiz E, Tomsia AP. Ice-templated porous alumina structures. Acta Mater 2007;55:1965–74.
[41] Dorcheh AS, Abbasi M. Silica aerogel; synthesis, properties and characterization. J Mater Process Technol 2008;199:10–26.
[42] Nyström G, Fernández-Ronco MP, Bolisetty S, Mazzotti M, Mezzenga R. Amyloid templated gold aerogels. Adv Mater 2016;28:472–8.
[43] Jung SM, Preston DJ, Jung HY, Deng Z, Wang EN, Kong J. Porous Cu nanowire aerosponges from one-step assembly and their applications in heat dissipation. Adv Mater 2016;28:1413–9.
[44] Wei G, Ma PX. Nanostructured biomaterials for regeneration. Adv Funct Mater 2008;18:3566–82.
[45] Lai F, Huang Y, Zuo L, Gu H, Miao Y-E, Liu T. Electrospun nanofiber-supported carbon aerogel as a versatile platform toward asymmetric supercapacitors. J Mater Chem A 2016;4:15861–9.
[46] Xu T, Ding Y, Wang Z, Zhao Y, Wu W, Fong H, et al. Three-dimensional and ultralight sponges with tunable conductivity assembled from electrospun nanofibers for a highly sensitive tactile pressure sensor. J Mater Chem C 2017;5:10288–94.
[47] Jiang S, Uch B, Agarwal S, Greiner A. Ultralight, thermally insulating, compressible polyimide fiber assembled sponges. ACS Appl Mater Interfaces 2017;9:32308–15.
[48] Zhu J, Jiang S, Hou H, Agarwal S, Greiner A. Low density, thermally stable, and intrinsic flame retardant poly(bis(benzimidazo)benzophenanthroline-dione) sponge. Macromol Mater Eng 2018;303:1700615.
[49] Xu T, Wang Z, Ding Y, Xu W, Wu W, Zhu Z, et al. Ultralight electrospun cellulose sponge with super-high capacity on absorption of organic compounds. Carbohydr Polym 2018;179:164–72.
[50] Yao Q, Cosme JGL, Xu T, Miszuk JM, Picciani PHS, Fong H, et al. Three dimensional electrospun PCL/PLA blend nanofibrous scaffolds with significantly improved stem cells osteogenic differentiation and cranial bone formation. Biomaterials 2017;115:115–27.
[51] Chen W, Ma J, Zhu L, Morsi Y, Ei-Hamshary H, Al-Deyab SS, et al. Superelastic, superabsorbent and 3D nanofiber-assembled scaffold for tissue engineering. Colloids Surf B Biointerfaces 2016;142:165–72.
[52] Si Y, Wang X, Yan C, Yang L, Yu J, Ding B. Ultralight biomass-derived carbonaceous nanofibrous aerogels with superelasticity and high pressure-sensitivity. Adv Mater 2016;28:9512–8.
[53] Si Y, Wang L, Wang X, Tang N, Yu J, Ding B. Ultrahigh-water-content, superelastic, and shape-memory nanofiber-assembled hydrogels exhibiting pressure-responsive conductivity. Adv Mater 2017;29:1700339.
[54] Huang Y, Lai F, Zhang L, Lu H, Miao Y-E, Liu T. Elastic carbon aerogels reconstructed from electrospun nanofibers and graphene as three-dimensional networked matrix for efficient energy storage/conversion. Sci Rep 2016;6:31541.
[55] Chen J, Zhang T, Hua W, Li P, Wang X. 3D Porous poly(lactic acid)/regenerated cellulose composite scaffolds based on electrospun nanofibers for biomineralization. Colloids Surf Physicochem Eng Aspects 2020;585:124048.
[56] Zhang S-J, Yu H-Q, Feng H-M. PVA-based activated carbon fibers with lotus root-like axially porous structure. Carbon 2006;44:2059–68.
[57] Zhang SJ, Feng HM, Wang JP, Yu HQ. Structure evolution and optimization in the fabrication of PVA-based activated carbon fibers. J Colloid Interface Sci 2008;321:96–102.
[58] Nagamine S, Matsumoto T, Hikima Y, Ohshima M. Fabrication of porous carbon nanofibers by phosphate-assisted carbonization of electrospun poly(vinyl alcohol) nanofibers. Mater Res Bull 2016;79:8–13.

[59] Jiang S, Helfricht N, Papastavrou G, Greiner A, Agarwal S. Low-density self-assembled poly(N-Isopropyl Acrylamide) sponges with ultrahigh and extremely fast water uptake and release. Macromol Rapid Commun 2018;39:1700838.
[60] Qian Z, Wang Z, Chen Y, Tong S, Ge M, Zhao N, et al. Superelastic and ultralight polyimide aerogels as thermal insulators and particulate air filters. J Mater Chem A 2018;6:828–32.
[61] Shen Y, Li D, Deng B, Liu Q, Liu H, Wu T. Robust polyimide nano/microfibre aerogels welded by solvent-vapour for environmental applications. Royal Soc Open Sci 2019;6:190596.
[62] Si Y, Fu Q, Wang X, Zhu J, Yu J, Sun G, et al. Superelastic and superhydrophobic nanofiber-assembled cellular aerogels for effective separation of oil/water emulsions. ACS Nano 2015;9:3791–9.
[63] Jiang S, Reich S, Uch B, Hu P, Agarwal S, Greiner A. Exploration of the electrical conductivity of double-network silver nanowires/polyimide porous low-density compressible sponges. ACS Appl Mater Interfaces 2017;9:34286–93.
[64] Duan G, Koehn-Serrano M, Greiner A. Highly efficient reusable sponge-type catalyst carriers based on short electrospun fibers. Macromol Rapid Commun 2017;38:1600511.
[65] Xu T, Zheng F, Chen Z, Ding Y, Liang Z, Liu Y, et al. Halloysite nanotubes sponges with skeletons made of electrospun nanofibers as innovative dye adsorbent and catalyst support. Chem Eng J 2019;360:280–8.
[66] Cheong JY, Benker L, Zhu J, Youn D-Y, Hou H, Agarwal S, et al. Generalized and feasible strategy to prepare ultra-porous, low density, compressible carbon nanoparticle sponges. Carbon 2019;154:363–9.
[67] Duan G, Jiang S, Moss T, Agarwal S, Greiner A. Ultralight open cell polymer sponges with advanced properties by PPX CVD coating. Polym Chem 2016;7:2759–64.
[68] Xu T, Liang Z, Ding B, Feng Q, Fong H. Polymer blend nanofibers containing polycaprolactone as biocompatible and biodegradable binding agent to fabricate electrospun three-dimensional scaffolds/structures. Polymer 2018;151:299–306.
[69] Xu T, Yao Q, Miszuk JM, Sanyour HJ, Hong Z, Sun H, et al. Tailoring weight ratio of PCL/PLA in electrospun three-dimensional nanofibrous scaffolds and the effect on osteogenic differentiation of stem cells. Colloids Surf B Biointerfaces 2018;171:31–9.
[70] Choi DJ, Choi SM, Kang HY, Min H-J, Lee R, Ikram M, et al. Bioactive fish collagen/polycaprolactone composite nanofibrous scaffolds fabricated by electrospinning for 3D cell culture. J Biotechnol 2015;205:47–58.
[71] Zheng R, Duan H, Xue J, Liu Y, Feng B, Zhao S, et al. The influence of Gelatin/PCL ratio and 3-D construct shape of electrospun membranes on cartilage regeneration. Biomaterials 2014;35:152–64.
[72] Lee H, Jang CH, Kim GH. A polycaprolactone/silk-fibroin nanofibrous composite combined with human umbilical cord serum for subacute tympanic membrane perforation; an in vitro and in vivo study. J Mater Chem B 2014;2:2703–13.
[73] Joshi MK, Tiwari AP, Pant HR, Shrestha BK, Kim HJ, Park CH, et al. In situ generation of cellulose nanocrystals in polycaprolactone nanofibers: effects on crystallinity, mechanical strength, biocompatibility, and biomimetic mineralization. ACS Appl Mater Interfaces 2015;7:19672–83.
[74] Fukunishi T, Best CA, Sugiura T, Shoji T, Yi T, Udelsman B, et al. Tissue-engineered small diameter arterial vascular grafts from cell-free nanofiber PCL/chitosan scaffolds in a sheep model. PLoS ONE 2016;11:e0158555.
[75] Ding Y, Yao Q, Li W, Schubert DW, Boccaccini AR, Roether JA. The evaluation of physical properties and in vitro cell behavior of PHB/PCL/sol-gel derived silica hybrid scaffolds and PHB/PCL/fumed silica composite scaffolds. Colloids Surf B Biointerfaces 2015;136:93–8.
[76] Antonova LV, Sevostyanova VV, Kutikhin AG, Mironov AV, Krivkina EO, Shabaev AR, et al. Vascular endothelial growth factor improves physico-mechanical properties and enhances endothelialization of poly(3-hydroxybutyrate-co-3-hydroxyvalerate)/poly(epsilon-caprolactone) small-diameter vascular grafts in vivo. Front Pharmacol 2016;7:230.
[77] Diez-Pascual AM, Diez-Vicente AL. Electrospun fibers of chitosan-grafted polycaprolactone/poly(3-hydroxybutyrate-co-3-hydroxyhexanoate) blends. J Mater Chem B 2016;4:600–12.
[78] Spearman SS, Irin F, Rivero IV, Green MJ, Abidi N. Effect of dsDNA wrapped single-walled carbon nanotubes on the thermal and mechanical properties of polycaprolactone and polyglycolide fiber blend composites. Polymer 2015;56:476–81.
[79] Zhao X, Luo J, Fang C, Xiong J. Investigation of polylactide/poly(epsilon-caprolactone)/multi-walled carbon nanotubes electrospun nanofibers with surface texture. RSC Adv 2015;5:99179–87.
[80] Jensen T, Blanchette A, Vadasz S, Dave A, Canfarotta M, Sayej WN, et al. Biomimetic and synthetic esophageal tissue engineering. Biomaterials 2015;57:133–41.
[81] Masoumi N, Annabi N, Assmann A, Larson BL, Hjortnaes J, Alemdar N, et al. Tri-layered elastomeric scaffolds for engineering heart valve leaflets. Biomaterials 2014;35:7774–85.
[82] Pfeiffer D, Stefanitsch C, Wankhammer K, Müller M, Dreyer L, Krolitzki B, et al. Endothelialization of electrospun polycaprolactone (PCL) small caliber vascular grafts spun from different polymer blends. J Biomed Mater Res A 2014;102:4500–9.
[83] Han D, Steckl AJ. Triaxial electrospun nanofiber membranes for controlled dual release of functional molecules. ACS Appl Mater Interfaces 2013;5:8241–5.
[84] Ku SH, Lee SH, Park CB. Synergic effects of nanofiber alignment and electroactivity on myoblast differentiation. Biomaterials 2012;33:6098–104.
[85] El-Fiqi A, Kim J-H, Kim H-W. Osteoinductive fibrous scaffolds of biopolymer/mesoporous bioactive glass nanocarriers with excellent bioactivity and long-term delivery of osteogenic drug. ACS Appl Mater Interfaces 2015;7:1140–52.
[86] Fu S, Ni P, Wang B, Chu B, Peng J, Zheng L, et al. In vivo biocompatibility and osteogenesis of electrospun poly(ε-caprolactone)–poly(ethylene glycol)–poly(ε-caprolactone)/nano-hydroxyapatite composite scaffold. Biomaterials 2012;33:8363–71.
[87] Baykan E, Koc A, Elcin AE, Elcin YM. Evaluation of a biomimetic poly(epsilon-caprolactone)/beta-tricalcium phosphate multispiral scaffold for bone tissue engineering: In vitro and in vivo studies. Biointerphases 2014;9:029011.
[88] Yu W, Jiang X, Cai M, Zhao W, Ye D, Zhou Y, et al. A novel electrospun nerve conduit enhanced by carbon nanotubes for peripheral nerve regeneration. Nanotechnology 2014;25:165102.
[89] Song J, Gao H, Zhu G, Cao X, Shi X, Wang Y. The preparation and characterization of polycaprolactone/graphene oxide biocomposite nanofiber scaffolds and their application for directing cell behaviors. Carbon 2015;95:1039–50.
[90] Si JH, Cui ZX, Wang QT, Liu Q, Liu CT. Biomimetic composite scaffolds based on mineralization of hydroxyapatite on electrospun poly(epsilon-caprolactone)/nanocellulose fibers. Carbohydr Polym 2016;143:270–8.
[91] Ji Y, Liang K, Shen X, Bowlin GL. Electrospinning and characterization of chitin nanofibril/polycaprolactone nanocomposite fiber mats. Carbohydr Polym 2014;101:68–74.
[92] Xue J, Niu Y, Gong M, Shi R, Chen D, Zhang L, et al. Electrospun microfiber membranes embedded with drug-loaded clay nanotubes for sustained antimicrobial protection. ACS Nano 2015;9:1600–12.
[93] Chen C-H, Chen S-H, Shalumon KT, Chen J-P. Dual functional core-sheath electrospun hyaluronic acid/polycaprolactone nanofibrous membranes embedded with silver nanoparticles for prevention of peritendinous adhesion. Acta Biomater 2015;26:225–35.
[94] Singh RK, Patel KD, Lee JH, Lee E-J, Kim J-H, Kim T-H, et al. Potential of magnetic nanofiber scaffolds with mechanical and biological properties applicable for bone regeneration. PLoS ONE 2014;9:e91584.
[95] Augustine R, Dominic EA, Reju I, Kaimal B, Kalarikkal N, Thomas S. Electrospun polycaprolactone membranes incorporated with ZnO nanoparticles as skin substitutes with enhanced fibroblast proliferation and wound healing. RSC Adv 2014;4:24777.
[96] Miszuk JM, Xu T, Yao Q, Fang F, Childs JD, Hong Z, et al. Functionalization of PCL-3D electrospun nanofibrous scaffolds for improved BMP2-induced bone formation. Appl Mater Today 2018;10:194–202.
[97] Luickx N, Van den Vreken N, D'Oosterlinck W, Van der Schueren L, Declercq H, De Clerck K, et al. Optimization of the activation and nucleation steps in the precipitation of a calcium phosphate primer layer on electrospun poly(ε-caprolactone). J Biomed Mater Res A 2015;103:511–24.
[98] Jeon H, Kim G. Preparation and characterization of an electrospun polycaprolactone (PCL) fibrous mat and multi-layered PCL scaffolds having a nanosized pattern-surface for tissue regeneration. J Mater Chem B 2014;2:171–80.

[99] Bhattacharjee P, Naskar D, Kim H-W, Maiti TK, Bhattacharya D, Kundu SC. Non-mulberry silk fibroin grafted PCL nanofibrous scaffold: Promising ECM for bone tissue engineering. Eur Polym J 2015;71:490–509.
[100] Li Q, Wang Z, Zhang S, Zheng W, Zhao Q, Zhang J, et al. Functionalization of the surface of electrospun poly(epsilon-caprolactone) mats using zwitterionic poly (carboxybetaine methacrylate) and cell-specific peptide for endothelial progenitor cells capture. Mater Sci Eng C 2013;33:1646–53.
[101] Wang JY, Wang K, Gu X, Luo Y. Polymerization of hydrogel network on microfiber surface: synthesis of hybrid water-absorbing matrices for biomedical applications. ACS Biomater Sci Eng 2016;2:887–92.
[102] Kang J, Yoo HS. Nucleic acid-scavenging electrospun nanofibrous meshes for suppressing inflammatory responses. Biomacromolecules 2014;15:2600–6.
[103] Fu H-L, Hong Y, Little SR, Wagner WR. Collagenase-labile polyurethane urea synthesis and processing into hollow fiber membranes. Biomacromolecules 2014;15:2924–32.
[104] Selvakumar M, Pawar HS, Francis NK, Das B, Dhara S, Chattopadhyay S. Excavating the role of aloe vera wrapped mesoporous hydroxyapatite frame ornamentation in newly architectured polyurethane scaffolds for osteogenesis and guided bone regeneration with microbial protection. ACS Appl Mater Interfaces 2016;8:5941–60.
[105] Hsu S-h, Hsieh C-T, Sun Y-M. Synthesis and characterization of waterborne polyurethane containing poly(3-hydroxybutyrate) as new biodegradable elastomers. J Mater Chem B 2015;3:9089–97.
[106] Vaquette C, Ivanovski S, Hamlet SM, Hutmacher DW. Effect of culture conditions and calcium phosphate coating on ectopic bone formation. Biomaterials 2013;34:5538–51.
[107] Croisier F, Atanasova G, Poumay Y, Jérôme C. Polysaccharide-coated PCL nanofibers for wound dressing applications. Adv Healthc Mater 2014;3:2032–9.
[108] Ku SH, Park CB. Human endothelial cell growth on mussel-inspired nanofiber scaffold for vascular tissue engineering. Biomaterials 2010;31:9431–7.
[109] Deng Y, Yang YY, Wei SC. Peptide-decorated nanofibrous niche augments in vitro directed osteogenic conversion of human pluripotent stem cells. Biomacromolecules 2017;18:587–98.
[110] Lee J, Yoo JJ, Atala A, Lee SJ. The effect of controlled release of PDGF-BB from heparin-conjugated electrospun PCL/gelatin scaffolds on cellular bioactivity and infiltration. Biomaterials 2012;33:6709–20.
[111] Kobsa S, Kristofik NJ, Sawyer AJ, Bothwell ALM, Kyriakides TR, Saltzman WM. An electrospun scaffold integrating nucleic acid delivery for treatment of full-thickness wounds. Biomaterials 2013;34:3891–901.
[112] Deuber F, Mousavi S, Hofer M, Adlhart C. Tailoring pore structure of ultralight electrospun sponges by solid templating. Chem Select 2016;1:5595–8.
[113] Deuber F, Mousavi S, Federer L, Adlhart C. Amphiphilic nanofiber-based aerogels for selective liquid absorption from electrospun biopolymers. Adv Mater Interfaces 2017;4:1700065.
[114] Kim JG, Choi TJ, Chang JY. Homogenized electrospun nanofiber reinforced microporous polymer sponge. Chem Eng J 2016;306:242–50.
[115] Kim T-W, Park S-J. Synthesis of reduced graphene oxide/thorn-like titanium dioxide nanofiber aerogels with enhanced electrochemical performance for supercapacitor. J Colloid Interface Sci 2017;486:287–95.
[116] Xiao J, Lv W, Song Y, Zheng Q. Graphene/nanofiber aerogels: Performance regulation towards multiple applications in dye adsorption and oil/water separation. Chem Eng J 2018;338:202–10.
[117] Alshrah M, Naguib HE, Park CB. Reinforced resorcinol formaldehyde aerogel with co-assembled polyacrylonitrile nanofibers and graphene oxide nanosheets. Mater Des 2018;151:154–63.
[118] Zhao X, Yang F, Wang Z, Ma P, Dong W, Hou H, et al. Mechanically strong and thermally insulating polyimide aerogels by homogeneity reinforcement of electrospun nanofibers. Compos Part B: Eng 2020;182:107624.
[119] Jiang S, Reich S, Uch B, Hu P, Agarwal S, Greiner A. Exploration of the electrical conductivity of double network silver nanowires–polyimide porous low density compressible sponges. ACS Appl Mater Interfaces 2017;9:34286–93.
[120] Si Y, Wang X, Dou L, Yu J, Ding B. Ultralight and fire-resistant ceramic nanofibrous aerogels with temperature-invariant superelasticity. Sci Adv 2018;4:eaas8925.
[121] Chen W, Chen S, Morsi Y, El-Hamshary H, El-Newhy M, Fan C, et al. Superabsorbent 3D scaffold based on electrospun nanofibers for cartilage tissue engineering. ACS Appl Mater Interfaces 2016;8:24415–25.
[122] Sun B, Zhou Z, Wu T, Chen W, Li D, Zheng H, et al. Development of nanofiber sponges-containing nerve guidance conduit for peripheral nerve regeneration in vivo. ACS Appl Mater Interfaces 2017;9:26684–96.
[123] Weng L, Boda SK, Wang H, Teusink MJ, Shuler FD, Xie J. Novel 3D hybrid nanofiber aerogels coupled with BMP-2 peptides for cranial bone regeneration. Adv Healthc Mater 2018;7:1701415.
[124] Xue Z, Cao Y, Liu N, Feng L, Jiang L. Special wettable materials for oil/water separation. J Mater Chem A 2014;2:2445–60.
[125] Chu Z, Feng Y, Seeger S. Oil/water separation with selective superantiwetting/superwetting surface materials. Angew Chem Int Ed 2015;54:2328–38.
[126] Wang B, Liang W, Guo Z, Liu W. Biomimetic super-lyophobic and super-lyophilic materials applied for oil/water separation: a new strategy beyond nature. Chem Soc Rev 2015;44:336–61.
[127] Ma Q, Cheng H, Fane AG, Wang R, Zhang H. Recent development of advanced materials with special wettability for selective oil/water separation. Small 2016;12:2186–202.
[128] Lu J, Xu D, Wei J, Yan S, Xiao R. Superoleophilic and flexible thermoplastic polymer nanofiber aerogels for removel of oils and organic solvents. ACS Appl Mater Interfaces 2017;9:25533–41.
[129] Jiang S, Duan G, Kuhn U, Mörl M, Altstädt V, Yarin AL, et al. Spongy gels by a top-down approach from polymer fibrous sponges. Angew Chem Int Ed 2017;56:3285–8.
[130] Liu L, Wan Y, Xie Y, Zhai R, Zhang B, Liu J. The removal of dye from aqueous solution using alginate-halloysite nanotube beads. Chem Eng J 2012;187:210–6.
[131] Mousavi S, Deuber F, Petrozzi S, Federer L, Aliabadi M, Shahraki F, et al. Efficient dye adsorption by highly porous nanofiber aerogels. Colloids Surf A 2018;547:117–25.
[132] Wang M, Li X, Hua W, Shen L, Yu X, Wang X. Electrospun poly(acrylic acid)/silica hydrogel nanofibers scaffold for highly efficient adsorption of lanthanide ions and its photoluminescence performance. ACS Appl Mater Interfaces 2016;8:23995–4007.
[133] Sun Y, Wu Z-Y, Wang X, Ding C, Cheng W, Yu S-H, et al. Macroscopic and microscopic investigation of U(VI) and Eu(III) adsorption on carbonaceous nanofibers. Environ Sci Technol 2016;50:4459–67.
[134] Wang M, Li X, Hua W, Deng L, Li P, Zhang T, et al. Superelastic three-dimensional nanofiber-reconfigured spongy hydrogels with superior adsorption of lanthanide ions and photoluminescence. Chem Eng J 2018;348:95–108.
[135] Deuber F, Mousavi S, Federeer L, Hofer M, Adlhart C. Exploration of ultralight nanofiber aerogels as particle filters: capacity and efficiency. ACS Appl Mater Interfaces 2018;10:9069–76.
[136] Fu Q, Si Y, Duan C, Yan Z, Liu L, Yu J, et al. Highly carboxylated, cellular structured, and underwater superelastic nanofibrous aerogels for efficient protein separation. Adv Funct Mater 2019;29:1808234.
[137] Fu Q, Liu L, Si Y, Yu J, Ding B. Shapeable, underwater superelastic, and highly phosphorylated nanofibrous aerogels for large-capacity and high-throughput protein separation. ACS Appl Mater Interfaces 2019;11:44874–85.
[138] Wang G, Zhang L, Zhang J. A review of electrode materials for electrochemical supercapacitors. Chem Soc Rev 2012;41:797–828.
[139] Yan J, Wang Q, Wei T, Fan Z. Recent advances in design and fabrication of electrochemical supercapacitors with high energy densities. Adv Energy Mater 2014;4:1300816.
[140] Zhao Y, Liu B, Pan L, Yu G. 3D nanostructured conductive polymer hydrogels for high-performance electrochemical devices. Energy Environ Sci 2013;6:2856–70.
[141] Lu XF, Wang C, Favier F, Pinna N. Electrospun nanomaterials for supercapacitor electrodes: designed architectures and electrochemical performance. Adv Energy Mater 2017;7:1601301.
[142] Zhang M, Yang D, Zhang S, Xu T, Shi Y, Liu Y, et al. Elastic and hierarchical carbon nanofiber aerogels and their hybrids with carbon nanotubes and cobalt oxide

nanoparticles for high-performance asymmetric supercapacitors. Carbon https://doi.org/10.1016/j.carbon.2019.11.071.
[143] Sun B, Long Y-Z, Chen Z-J, Liu S-L, Zhang H-D, Zhang J-C, et al. Recent advances in flexible and stretchable electronic devices via electrospinning. J Mater Chem C 2014;2:1209–19.
[144] Wang X, Dong L, Zhang H, Yu R, Pan C, Wang ZL. Recent progress in electronic skin. Adv Sci 2015;2:1500169.
[145] Bandodkar AJ, Jeerapan I, Wang J. Wearable chemical sensors: Present challenges and future prospects. ACS Sens 2016;1:464–82.
[146] Trung TQ, Lee N-E. Materials and devices for transparent stretchable electronics. J Mater Chem C 2017;5:2202–22.
[147] Zhao S, Li J, Cao D, Zhang G, Li J, Li K, et al. Recent advancements in flexible and stretchable electrodes for electromechanical sensors: strategies, materials, and features. ACS Appl Mater Interfaces 2017;9:12147–64.
[148] Zou J, Liu J, Karakoti AS, Kumar A, Joung D, Li Q, et al. Ultralight multiwalled carbon nanotube aerogel. ACS Nano 2010;4:7293–302.
[149] Zhao S, Zhang G, Gao Y, Deng L, Li J, Sun R, et al. Strain-driven and ultrasensitive resistive sensor/switch based on conductive alginate/nitrogen-doped carbon-nanotube-supported Ag hybrid aerogels with pyramid design. ACS Appl Mater Interfaces 2014;6:22823–9.
[150] Kuang J, Liu L, Gao Y, Zhou D, Chen Z, Han B, et al. A hierarchically structured graphene foam and its potential as a large-scale strain-gauge sensor. Nanoscale 2013;5:12171–7.
[151] Qin Y, Peng Q, Ding Y, Lin Z, Wang C, Li Y, et al. Lightweight, superelastic, and mechanically flexible graphene/polyimide nanocomposite foam for strain sensor application. ACS Nano 2015;9:8933–41.
[152] Hou X, Zhang R, Fang D. Superelastic, fatigue resistant and heat insulated carbon nanofiber aerogels for piezoresistive stress sensors. Ceram Int 2020;46:2122–7.
[153] Massaro M, Colletti CG, Lazzara G, Milioto S, Noto R, Riela S. Halloysite nanotubes as support for metal-based catalysts. J Mater Chem A 2017;5:13276–93.
[154] Wang H, Zhang X, Wang N, Li Y, Feng X, Huang Y, et al. Ultralight, scalable, and high-temperature–resilient ceramic nanofiber sponges. Sci Adv 2017;3:e1603170.
[155] Dou L, Zhang X, Cheng X, Ma Z, Wang X, Si Y, et al. Hierarchical cellular structured ceramic nanofibrous aerogels with temperature-invariant superelasticity for thermal insulation. ACS Appl Mater Interfaces 2019;11:29056–64.
[156] Petite H, Viateau V, Bensaïd W, Meunier A, de Pollak C, Bourguignon M, et al. Tissue-engineered bone regeneration. Nat Biotechnol 2000;18:959–63.
[157] Bose S, Roy M, Bandyopadhyay A. Recent advances in bone tissue engineering scaffolds. Trends Biotechnol 2012;30:546–54.
[158] Rezwan K, Chen Q, Blaker J, Boccaccini AR. Biodegradable and bioactive porous polymer/inorganic composite scaffolds for bone tissue engineering. Biomaterials 2006;27:3413–31.
[159] Hollister SJ. Porous scaffold design for tissue engineering. Nat Mater 2005;4:518–24.
[160] Badylak SF, Freytes DO, Gilbert TW. Extracellular matrix as a biological scaffold material: structure and function. Acta Biomater 2009;5:1–13.
[161] Venkatesan J, Kim SK. Nano-hydroxyapatite composite biomaterials for bone tissue engineering-a review. J Biomed Nanotechnol 2014;10:3124–40.
[162] Wang J, Chen Y, Zhu X, Yuan T, Tan Y, Fan Y, et al. Effect of phase composition on protein adsorption and osteoinduction of porous calcium phosphate ceramics in mice. J Biomed Mater Res A 2014;102:4234–43.
[163] He X, Liu Y, Yuan X, Lu L. Enhanced healing of rat calvarial defects with MSCs loaded on BMP-2 releasing chitosan/alginate/hydroxyapatite scaffolds. PLoS ONE 2014;9:e104061.
[164] Park KW, Waki H, Kim WK, Davies BS, Young SG, Parhami F, et al. The small molecule phenamil induces osteoblast differentiation and mineralization. Mol Cell Biol 2009;29:3905–14.
[165] Fan J, Im CS, Cui ZK, Guo M, Bezouglaia O, Fartash A, et al. Delivery of phenamil enhances BMP-2-induced osteogenic differentiation of adipose-derived stem cells and bone formation in calvarial defects. Tissue Eng Part A 2015;21:2053–65.
[166] Lo KW, Ulery BD, Kan HM, Ashe KM, Laurencin CT. Evaluating the feasibility of utilizing the small molecule phenamil as a novel biofactor for bone regenerative engineering. J Tissue Eng Regen Med 2014;8:728–36.
[167] Wang L, Qiu Y, Lv H, Si Y, Liu L, Zhang Q, et al. 3D superelastic scaffolds constructed from flexible inorganic nanofibers with self-fitting capability and tailorable gradient for bone regeneration. Adv Funct Mater 2019;29:1901407.
[168] Wang L, Qiu Y, Guo Y, Si Y, Liu L, Cao J, et al. Smart, elastic, and nanofiber-based 3D scaffolds with self-deploying capability for osteoporotic bone regeneration. Nano Lett 2019;19:9112–20.
[169] Suh J-KF, Matthew HW. Application of chitosan-based polysaccharide biomaterials in cartilage tissue engineering: a review. Biomaterials 2000;21:2589–98.
[170] Temenoff JS, Mikos AG. Tissue engineering for regeneration of articular cartilage. Biomaterials 2000;21:431–40.
[171] Li Y, Liu Y, Xun X, Zhang W, Xu Y, Gu D. Three-dimensional porous scaffolds with biomimetic microarchitecture and bioactivity for cartilage tissue engineering. ACS Appl Mater Interfaces 2019;11:36359–70.
[172] Cao H, Liu T, Chew SY. The application of nanofibrous scaffolds in neural tissue engineering. Adv Drug Del Rev 2009;61:1055–64.
[173] Xie J, MacEwan MR, Schwartz AG, Xia Y. Electrospun nanofibers for neural tissue engineering. Nanoscale 2010;2:35–44.
[174] Peppas NA, Hilt JZ, Khademhosseini A, Langer R. Hydrogels in biology and medicine: from molecular principles to bionanotechnology. Adv Mater 2006;18:1345–60.
[175] Slaughter BV, Khurshid SS, Fisher OZ, Khademhosseini A, Peppas NA. Hydrogels in regenerative medicine. Adv Mater 2009;21:3307–29.
[176] Kopeček J, Yang J. Smart self-assembled hybrid hydrogel biomaterials. Angew Chem Int Ed 2012;51:7396–417.
[177] Billiet T, Vandenhaute M, Schelfhout J, Van Vlierberghe S, Dubruel P. A review of trends and limitations in hydrogel-rapid prototyping for tissue engineering. Biomaterials 2012;33:6020–41.
[178] Fu Q, Duan C, Yan Z, Li Y, Si Y, Liu L, et al. Nanofiber-based hydrogels: controllable synthesis and multifunctional applications. Macromol Rapid Commun 2018;39:1800058.
[179] Duan G, Bagheri ARR, Jiang S, Golenser J, Agarwal S, Greiner A. Exploration of macroporous polymeric sponges as drug carriers. Biomacromolecules 2017;18:3215–21.
[180] Dao V-D, Choi H-S. Carbon-based sunlight absorbers in solar-driven steam generation devices. Global Challenges 2018;2:1700094.
[181] Xue J, Wu T, Dai Y, Xia Y. Electrospinning and electrospun nanofibers: Methods, materials, and applications. Chem Rev 2019;119:5298–415.

Dr. Tao Xu is a Postdoctoral Research Fellow in the Center for Nanotechnology and Nanotoxicology at the Harvard T.H. Chan School of Public Health, Harvard University (USA). He received his Ph.D. in Biomedical Engineering at the South Dakota School of Mines and Technology in 2018. His research interests include (1) electrospun 3D nanofibrous structures for biomedicine, energy, and environment applications, (2) nanoencapsulation and smart/responsive delivery of agrichemicals using electrospray/electrospinning of nature derived biopolymers, and (3) smart food packaging materials using electrospinning of nature derived biopolymers.

Dr. Yichun Ding is an Associate Professor at the Fujian Institute of Research on the Structure of Matter, Chinese Academy of Sciences (China). He received his Ph.D. in Biomedical Engineering at the South Dakota School of Mines and Technology in 2018. His research interests include (1) nanomaterials & nanostructures, (2) electrospinning & electrospun nanofibers, (3) flexible and wearable sensors for human health monitoring, (4) flexible electronics & energy storage/conversion devices, and (3) high performance aromatic polymers & conjugated/conducting polymers.

Mr. Zhipeng Liang is a Ph.D. student in Biomedical Engineering at the South Dakota School of Mines and Technology (USA). His dissertation research is focused on electrospun 3D nanofibrous scaffolds for bone tissue engineering application.

Dr. Hongli Sun is an Associate Professor in the Iowa Institute for Oral Health Research and the Department of Oral and Maxillofacial Surgery at the University of Iowa (USA). He received his Ph.D. in Cell Biology at the Shanghai Institute for Biological Sciences, Chinese Academy of Sciences (China) in 2007. Prior to joining the University of Iowa in 2018, he was an Assistant Professor in Biomedical Engineering at the University of South Dakota (2014-2018) and a Postdoctoral Fellow in

School of Dentistry at the University of Michigan (2007-2014). His research interests include (1) promote endogenous bone formation by developing bio-mimicking nanofibrous 3D scaffolds, (2) promote challenged bone repair by targeting angiogenesis/inflammation via local drug delivery (small molecule drugs), and (3) study the role of adult stem cells and 3D microenvironment in bone metastasis.

Dr. Fan Zheng is a Research Scientist in the Composites and Polymer Engineering (CAPE) Laboratory at the South Dakota School of Mines and Technology (USA). She received her Ph.D. in Nanoscience and Nanoengineering at the South Dakota School of Mines and Technology in 2018. Her research interests include (1) nanomaterial synthesis, (2) lithium-ion batteries, and (3) flexible electronics (*e.g.*, dye-sensitized solar cells).

Dr. Zhengtao Zhu is an Associate Professor in the Program of Biomedical Engineering at the South Dakota School of Mines and Technology (USA). He received his Ph.D. in Materials Chemistry from the State University of New York at Binghamton in 2002. Prior to joining the SDSM&T in 2006, he was a postdoctoral research associate at the Cornell University (2002-2004) and the University of Illinois at Urbana-Champaign (2004-2006). His research interests include (1) developing novel synthesis and fabrication methods, (2) understanding the structure-property relations of the hybrid materials at the nanometer scale, and (3) exploring the applications of these materials in flexible electronics and biomedical sensors.

Dr. Yong Zhao is a Senior Microscopy Specialist in the Keck Center for Advanced Microscopy and Microanalysis at the University of Delaware (USA). He received his Ph.D. in Chemistry at the University of Texas at El Paso in 2010. Prior to joining the University of Delaware in 2016, he was a Research Scientist in the Department of Chemistry and Applied Biological Sciences at the SDSM&T (2010-2016). His research interests include (1) preparation, characterization, and evaluation of polymeric, ceramic, metallic, and carbonaceous nanofibers via the nanomaterials-processing technique of electrospinning, (2) applications of electrospun nanofibrous materials including, but not limited to, composites, filtration/separation, biomedical engineering, electronic applications, and energy related applications, and (3) advanced SEM, TEM, STEM, and focused ion beam (FIB) microscopy.

Dr. Hao Fong is a (Full) Professor in the Department of Chemistry and Applied Biological Sciences at the SDSM&T, and he is also an important faculty member in the SDSM&T's multidisciplinary graduate programs of Materials Engineering and Science (MES), Biomedical Engineering (BME), and Nanoscience and Nanoengineering (NANO). Dr. Fong is one of the pioneers and a top scientist worldwide in the field of "Electrospinning and Nanofibers". He has published over 160 peer-reviewed journal articles, ~20 books and/or book chapters, and numerous symposium proceedings/presentations. According to *Google Scholar* (on October 5, 2019), his publications have been cited for 13,974 times; and his personal H-Index is 53. Dr. Fong's highest degree is a Ph.D. earned in 1999 from the Department of Polymer Science at the University of Akron (USA); and his Ph.D. advisor is Dr. Darrell H. Reneker, who re-vitalized the research on the technique of electrospinning in the1990's. In the recent 16 years, Dr. Hao Fong's research endeavors are focused on "The Technique of Electrospinning and Various Applications of Electrospun Polymer, Ceramic, Carbon/Graphite, Composite, and Hierarchically-structured Nanofibers and/or Nanofibrous Materials". The interested/studied applications include, but not limited to (1) filtration/separation applications (*e.g.*, separation of biopharmaceutical therapeutics such as proteins, water purification such as micro-/ultra-/nano-filtrations), (2) energy-related applications (*e.g.*, solar cells, batteries, fuel cells, and supercapacitors), (3) biomedical/biochemical applications (*e.g.*, tissue engineering, drug delivery, antimicrobial wound dressing, and enzyme immobilization), (4) microelectronics-related applications (*e.g.*, sensors/detectors and transistors), and (5) composite applications (*e.g.*, hybrid multi-scale composites and dental restorative composites).